Chapter 15
Unmyelinated and Myelinated Axons Exhibit Differential Injury and Treatment Responses Following Traumatic Injury

Thomas M. Reeves, Adele E. Doperalski, and Linda L. Phillips

Abbreviations

ACSF	Artificial cerebrospinal fluid
APP	Amyloid precursor protein
BBB	Blood–brain barrier
CAP	Compound action potential
CC	Corpus callosum
CsA	Cyclosporin-A
DAI	Diffuse axonal injury
DTI	Diffusion tensor imaging
FPI	Fluid percussion injury
HRP	Horseradish peroxidase
IC	Internal capsule
IPI	Interpulse interval
MMP	Matrix metalloproteinase
MS	Multiple sclerosis
N1	CAP generated by myelinated axons
N2	CAP generated by unmyelinated axons
TAI	Traumatic axonal injury
TBI	Traumatic brain injury

Over 1.5 million new traumatic brain injury (TBI) cases are reported annually in the U.S. alone (Rutland-Brown et al. 2006), leading to an enduring public health problem and persistent challenges in patients' lives. Experimental and clinical evidence

T.M. Reeves, Ph.D. (✉) • A.E. Doperalski, Ph.D. • L.L. Phillips
Department of Anatomy and Neurobiology, Virginia Commonwealth University,
P.O. Box 980709, Richmond, VA 23298, USA
e-mail: tmreeves@vcu.edu

S. Baltan et al. (eds.), *White Matter Injury in Stroke and CNS Disease*, Springer Series in Translational Stroke Research 4, DOI 10.1007/978-1-4614-9123-1_15,

reveals TBI as a complex and multifaceted pathology, affecting widespread cellular and vascular systems (for reviews: Graham et al. 2000; Phillips and Reeves 2001; Leker and Shohami 2002; Povlishock and Katz 2005; Park et al. 2008). Despite these complexities, it has become clear that axons are among the most vulnerable, and the most commonly injured, cellular components in the nervous system (Adams et al. 1989; Maxwell et al. 1997; Povlishock 1992; Smith and Meaney 2000). Axonal injury is a concomitant of most TBIs requiring hospitalization. Diffuse axonal injury (DAI) was recently observed to occur in 72 % of patients with moderate or severe TBI, and was associated with worse outcome (Skandsen et al. 2010). This diffuse pathology is also associated with posttraumatic coma, and persistent memory deficits with impaired information processing capacity (Meythaler et al. 2001).

Research has identified key aspects of traumatic axonal injury and established that the pathology is multiphasic, with a rapid primary injury phase, including a failure of ionic homeostasis, evolving over hours and days to a more protracted secondary injury phase involving aberrant biochemical cascades and proteolysis. Research findings in recent years have led to significant advances towards an understanding of the pathogenetic mechanisms in traumatic axonal injury, but many questions remain unanswered.

A fundamental gap, in the knowledge-base pertaining to traumatic axonal injury, is uncertainty regarding whether all axons respond to injury in the same way. Currently there is only sparse information regarding how axon phenotype influences the extent of injury and the capacity for recovery, and this impedes progress towards a comprehensive understanding of the pathomechanisms of axonal injury while limiting the search for new therapeutic strategies. The following discussion reviews evidence, accumulated using experimental animal models of TBI, indicating that separate populations of axons undergo distinctive responses to injury, and to treatment with neuroprotective compounds. The presence or absence of myelin is one phenotypic dimension on which axons may be classified into discrete populations. As an initial approach to study how axon type influences the injury process, our laboratory has investigated how unmyelinated axons undergo an injury response distinct from that of myelinated axons.

This chapter first considers the conceptual basis for predicting an elevated risk to traumatic injury in the unmyelinated axon population. This is followed by a summary of quantitative ultrastructural evidence of fiber-type-specific changes in morphology observed in corpus callosum (CC) axons following TBI. Next, we describe electrophysiological findings which document dissimilar conduction deficits in the unmyelinated and myelinated axon populations, and differential degrees of responsiveness to neuroprotective compounds. Subsequently, we discuss a set of results which demonstrate the critical role of the extracellular matrix in axonal posttraumatic sequelae, and how the unmyelinated fiber interaction with matrix elements may diverge from that of myelinated fibers. Finally, we describe initial results in a new line of inquiry, recently undertaken in our laboratory, to contrast axonal injury in white matter having mixed unmyelinated and myelinated axons, the CC, with that of the internal capsule, which is predominantly composed of myelinated axons.

15.1 Intrinsic Axon Properties Influence Vulnerability

The conceptual framework, regarding mechanisms of axonal injury following closed head (nonpenetrating) injury, has evolved beyond the once prevalent notion that axon death is due mainly to shear and tensile forces acting at the moment of injury (Strich 1961). It is now well established that, at least for myelinated CNS axons, most injured fibers undergo a progressive secondary pathology involving cytoskeletal changes, impaired axoplasmic transport, and axonal swelling (Povlishock and Christman 1995; Maxwell et al. 1997; Saatman et al. 1998; Smith et al. 1998). However, more recent studies provided indirect evidence for subpopulations of axons which undergo different forms of the secondary injury response. Some injured axons exhibited neurofilament compaction independently of impaired fast transport (Stone et al. 2001; DiLeonardi et al. 2009). Moreover, the degree to which these two pathological components were both expressed in individual axons was determined, in part, by axon caliber and anatomical location. Larger medial lemniscal fibers exhibited both pathologies concurrently to a greater extent than was the case for smaller corticospinal axons (Stone et al. 2001), and treatment with the immunophilin ligand FK506 differentially attenuated these abnormalities (Marmarou and Povlishock 2006). Other workers, using an in vivo optic-nerve stretch model of injury, reported that caliber of the myelinated axons was associated with several pathological parameters of axonal injury, including the degree of neurofilament and microtubule damage (Jafari et al. 1997, 1998). In a morphological study of the CC of nonhuman primates, axolemmal tearing was observed to occur selectively at the nodes of small, thinly-myelinated axons (Maxwell et al. 1993). These diverse findings converge on the idea that intrinsic properties of axons, especially axon caliber, are important determinants of the severity of posttraumatic pathology. This presents a contrast to prevailing concepts of axonal injury as an undifferentiated pathology, present in varying degrees but generally affecting populations of axons indiscriminately.

15.1.1 Rationale for Predicting Elevated Risk to Unmyelinated Axons

There are both theoretical and empirical reasons for predicting that differences in fiber size, and the presence or absence of myelin, are likely to be critical factors in the injury processes affecting axons. Figure 15.1 suggests how fundamental physical differences between unmyelinated vs. myelinated axons are predicted to affect the course of pathological events following TBI. Myelin itself may exert a protective benefit in at least two ways. First, layers of myelin may provide physical support and function as a protective cushion at the instant of injury, reducing the mechanical forces acting on underlying axolemma. Secondly, myelin may shield underlying axolemmal membrane from the aberrant extracellular milieu known to

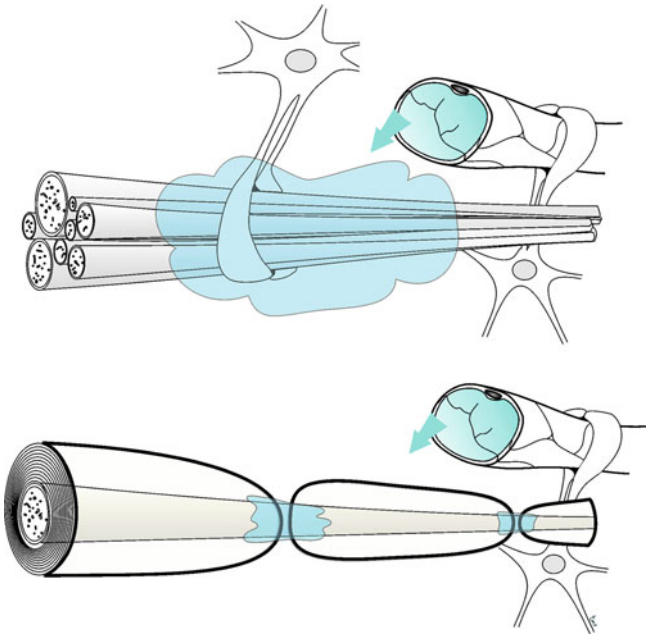

Fig. 15.1 Morphological properties of unmyelinated axons may place them at elevated risk to TBI. Diagram of unmyelinated axons, and a myelinated axon, in relation to nonneuronal elements (blood vessels, astrocytes). Unmyelinated axolemma is more exposed, than myelinated, to destructive extracellular influences (*shading*) arising locally (e.g., ionic imbalances and activated proteases), or from blood-borne factors infiltrating through a compromised blood–brain barrier (*arrows*). These structural differences are likely to contribute to a greater vulnerability of unmyelinated axons in some injury conditions. From Reeves et al. 2012, with permission

prevail after neurotrauma, including ionic imbalances (Katayama et al. 1990), and destructive proteolysis (Hall et al. 2005; Saatman et al. 2010; Reeves et al. 2010). Figure 15.1 also conveys that these two types of fibers present strikingly different degrees of axolemmal exposure to deleterious blood-borne factors, known to gain parenchymal access subsequent to TBI-induced failure of the blood–brain barrier (Kelley et al. 2007; Morganti-Kossmann et al. 2007; Cederberg and Siesjo 2010). While the lack of myelin may constitute a risk factor for the unmyelinated fibers, it may, paradoxically, provide a treatment benefit to those same axons as neuroprotective drugs are developed and applied, because these compounds will have more access to the full length of axolemma in the unmyelinated population.

Based on their biophysical properties, we hypothesized that unmyelinated axons are at an elevated risk to TBI. Among all components of neuronal cytoarchitecture, axons are the subcellular compartment with the highest membrane-to-cytoplasm ratio, which likely renders them vulnerable to membrane-targeting pathomechanisms of TBI, including lipid peroxidation (Evans 1993; Xiong et al. 2007), rapid proteolysis of voltage-gated sodium channels (Iwata et al. 2004; von Reyn et al. 2009), and more protracted proteolytic events attacking submembrane ankyrin

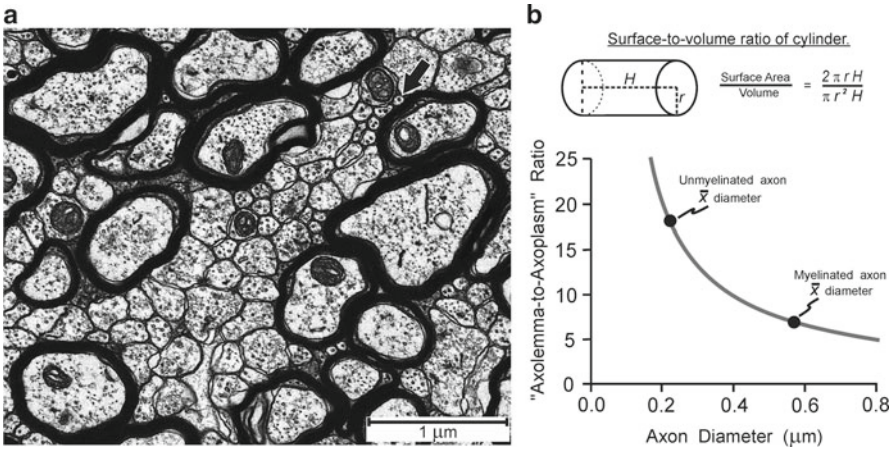

Fig. 15.2 Small diameter axons have a proportionately high membrane content. (**a**) Sample electron micrograph of CC axons in cross section, illustrating striking differences in size of unmyelinated and myelinated axons, with some unmyelinated diameters below 0.1 µm (*arrow*). (**b**) Modeling axons as uniform cylinders of arbitrary length, a decrease in diameter corresponds to an increase in surface-to-volume ratio. In cellular terms, an increased ratio of axolemma area to axoplasm volume, probably constitutes a risk to membrane-targeting TBI pathologies. In the *lower panel*, the mean diameters for unmyelinated and myelinated axons, measured in our laboratory, are plotted on the *curve* relating diameter to the surface-to-volume ratio. The mean diameter of unmyelinated axons is about 60 % smaller than the mean myelinated diameter, but this corresponds to an approximate 160 % increase in the surface-to-volume ratio. Panel B from Reeves et al. 2012, with permission

(Reeves et al. 2010) and spectrin (Hall et al. 2005; Saatman et al. 2003, 2010). In ultrastructural examination of CNS axons, the striking differences in scale of the unmyelinated and myelinated axons is readily apparent. Most of our recent observations in this regard have been directed at the CC of adult rats, and Fig. 15.2a shows an example micrograph of callosal axons in sagittal section, as they cross the midline. In an extensive stereological examination of these fibers (described below), we measured the mean diameter of the unmyelinated axons as 0.22 µm, and myelinated axons as 0.57 µm (axolemmal-bound region only, not including myelin layers). Unmyelinated axons at the smallest end of the size distribution present a cross-sectional appearance which is little more than a single microtubule with only a minimal volume of cytoplasm, corresponding to an extremely high membrane fraction. To quantify this relationship, Fig. 15.2b models axons as uniform cylinders of arbitrary length, and plots our measured values of mean axon diameter on the curve relating surface-to-volume ratio to diameter. It is notable that while the mean diameter of unmyelinated axons is about 60 % smaller than the mean myelinated diameter, this corresponds to a 160 % increase in the surface-to-volume ratio, or "axolemma-to-axoplasm" ratio as depicted in the graphic. There is reason to expect this substantial difference in cellular geometry affects the course of postinjury axonal pathology. Excessive elevation of intracellular calcium is widespread after TBI, and

this pathomechanism may especially challenge small axons with less cytoplasmic volume and calcium buffering/sequestration capacity, which is known to be critical in white matter injury (Stys 2004). These concepts formed the basis for our hypothesis that unmyelinated and myelinated axons would exhibit a differential vulnerability following an experimental TBI. The following material summarizes the methods and key results from those series of experiments.

15.2 Description of Injury Model

15.2.1 Midline Fluid Percussion Injury Model

The experimental TBI model selected for these studies was fluid percussion injury (FPI) in adult rats. This model was originally developed at our institution (Dixon et al. 1987), and has subsequently been extensively characterized and applied to a wide range of cellular pathologies initiated by neurotrauma (for recent reviews, Thompson et al. 2005; O'Connor et al. 2011; Reeves and Colley 2012). All procedures followed national guidelines for the care and use of experimental animals, and experimental protocols were approved by our institutional Animal Research Committee. For details of the FPI methodology readers are referred to the original reports summarized in this chapter (Colley et al. 2010; Reeves and Colley 2012; Reeves et al. 2005, 2007, 2010, 2012). In brief, FPI is induced by transiently injecting a small volume of saline into the epidural space through a 4.5 mm craniotomy, which deforms the brain tissue for a duration of approximately 20 ms. Injury severity is controlled by varying the pressure pulse magnitude, and the technique allows flexible craniotomy placement, to locate the pressure pulse over the cortical region of interest. In all experiments described here, FPI was applied at a moderate intensity (~2.0 atm.) to the brain midline, equidistant between bregma and lambda.

Our laboratory has consistently focused on TBI pathomechanisms related to sublethal changes in neurons. Cells which survive the primary-phase trauma will form the basis for subsequent functional recovery. In the case of axons, degenerating axons are not salvageable, but fibers which undergo time-dependent changes in structure and function form valid targets for intervention. The specific FPI parameters used for our studies (moderate intensity, midline location) induce a diffuse brain injury without contusion or hematoma, and without significant Wallerian degeneration. However, this injury does produce functional impairments, including suppression of axonal excitability (Baker et al. 2002; Reeves et al. 2005, 2007; Ai et al. 2007; Colley et al. 2010), and deficits in spatial cognition without hippocampal cell death (Lyeth et al. 1990). For these reasons, this injury model was well suited to investigate how unmyelinated axons exhibit postinjury structural and functional changes distinct from those seen in myelinated axons.

It must be emphasized that the changes we observe in axon function and structure are not an experimental form of the clinical condition of DAI. While the

most severe cases of DAI may be detected by computerized tomography and conventional magnetic resonance imaging, growing evidence indicates newer technologies, especially diffusion tensor imaging (DTI), provide a more accurate assessment of the pathology (reviewed by Li and Feng 2009). The microscopic features of DAI correspond to cytoskeletal and membrane disruptions, culminating in Wallerian-type axonal degeneration (Arfanakis et al. 2002). These dying axons do not participate in time-dependent functional recovery of white matter which we and others have documented to occur in animal TBI models. As detailed below, we observe TBI-induced axonal changes along multiple functional, structural, and molecular dimensions, which do not necessarily involve degeneration. Accordingly, to differentiate these observations from the more narrowly defined clinical DAI, the following discussion uses the term traumatic axonal injury (TAI) to indicate the full spectrum of structural and functional alterations affecting axons after TBI.

15.3 Quantitative Ultrastructure of Axonal Changes in Corpus Callosum Following TBI

15.3.1 Most Forebrain Axons are Unmyelinated

The vast majority of previous laboratory studies of TAI have focused on myelinated axons. This emphasis is understandable and reasonable from two perspectives. First, the existing knowledge-base pertaining to axonal injury is based largely on observations from heavily myelinated brainstem fiber tracts. Secondly, it was not recognized until recently that a surprisingly large proportion of cerebral axons are unmyelinated, and quantification of injury phenomena in these diminutive fibers presents technical challenges. In rodent injury models using impact acceleration or fluid percussion, TAI is most strongly expressed in brainstem fiber tracts such as the corticospinal tact and the medial longitudinal fasciculus, and is observed less frequently in cerebral sites. The brainstem tracts are predominantly comprised of comparatively large myelinated axons, and the proportion of pyramidal tract fibers which are unmyelinated was estimated as only ~20 % in earlier quantitative ultrastructural work (Samorajski and Friede 1968). No definitive explanation has been advanced to account for why the rodent TBI models more severely injure brainstem axons than more rostrally positioned axons. We speculate that mechanical forces may come to a focus as the rodent cranial vault narrows ventrally and posteriorly, and brainstem axons are compressed against bone rather than underlying soft tissue. Nevertheless, a rich body of knowledge has been generated through observations of posttraumatic sequential changes manifested in these fibers, usually evoked using impact acceleration injury models of TBI (e.g., Pettus et al. 1994; Povlishock 1992; Povlishock et al. 1997; Okonkwo et al. 1999; Buki et al. 1999, 2003; Singleton et al. 2001; Stone et al. 2001, 2002; Marmarou and Povlishock 2006).

These reports reveal time-dependent axon pathology beginning with focal axolemmal perturbations, probably mechanically induced at the instant of injury and associated with aberrant permeability. Subsequent stages involve microtubule loss, neurofilament alterations, axonal swelling, and scattered degenerating fibers.

Until 2003, quantitative data pertaining to the caliber and type of axons in the forebrain was only available for the CC. A study by Partadiredja and colleagues (2003) provided rigorous ultrastructural stereological assessments of fiber type and caliber in adult rat cerebral white matter, sampling frontal, parietal, and occipital regions at parasagittal sites chosen to minimize overlap with fibers of the CC (approximately 4.2 mm lateral from midline). Their results, based on systematic random sampling methods, showed that unmyelinated axons made up 76–90 % of axons, depending upon region sampled. Prior estimates of fiber composition in the rat CC have shown a historical trend. Earlier studies confined to the rodent splenium portion of the callosum estimated that about 45 % of axons were unmyelinated (e.g., Seggie and Berry 1972). More recent studies have consistently estimated the proportion of splenial axons which are unmyelinated to be about 88 % (Juraska and Kopcik 1988; Gravel et al. 1990; Kim et al. 1996). This recent consensus probably reflects sampling strategies which span the dorsal-to-ventral extent of the callosum, and thus avoid samples restricted to strata containing primarily a single fiber type.

The fact that the majority of forebrain axons are unmyelinated has ramifications for the field of TBI. If laboratory results point to distinctive pathophysiological responses in the unmyelinated population, then these should be assimilated into any comprehensive conceptual models of TAI. Equally important, if preclinical findings show unmyelinated and myelinated axons to have different responses to neuroprotective compounds (or different therapeutic temporal windows), then this information may usefully inform clinical trials targeting DAI.

15.3.2 A Measurement Focus on the Corpus Callosum

For both theoretical and practical reasons, we initially focused our studies of white matter injury on the CC. Clinical studies indicate the CC is particularly vulnerable to TBI, and some have attributed this vulnerability to the structure's unique anatomic location and composition (King et al. 1995; Gorrie et al. 2001). The presence of DAI in the CC was found to be more strongly predictive of poor outcome than even brainstem DAI (Rosa et al. 2011). The grave consequences of CC damage would be expected considering the multiple functions involving the structure, including transfer of lateralized verbal information, coordination of bilateral movements, and participation in cognitive and executive processes (Pandya et al. 1971; Geffen et al. 1994; Bhadelia et al. 2009). In the context of research using experimental rodent models of TBI, observations of the CC confer practical advantages. Because the CC is the largest white matter tract in the mammalian CNS, it presents a favorable site for replicable electrophysiological electrode placement, and selective dissections of the callosum provide sufficient tissue volume for molecular assays.

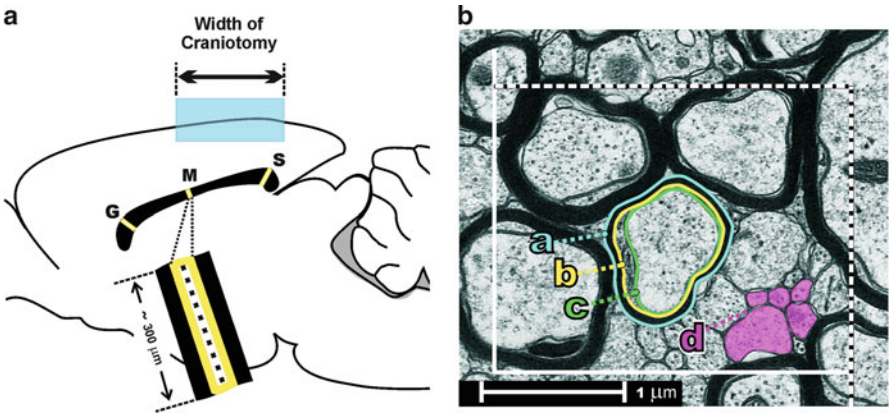

Fig. 15.3 (**a**) Midsagittal diagram of rat brain, showing stereological sampling scheme covering the dorsal-to-ventral extent of the CC at genu (G), mid-callosum (M), and splenium (S). *Shaded region* shows width and location of craniotomy for midline FPI. (**b**) Example of an unbiased stereological counting frame. *Shaded profiles* (*d*) show example unmyelinated axon profiles. Representative myelinated profile shows three contours were digitally traced for areal measurements: *a*, outer myelin border; *b*, inner myelin border; *c*, axolemma. From Reeves et al. 2012, with permission

15.3.3 Ultrastructural Stereology of Corpus Callosum Following FPI

Our laboratory assessed ultrastructural changes in CC of adult rats ($N=54$) at survival intervals ranging from 3 h to 15 days following midline FPI (Reeves et al. 2012). Some rats were given sham injuries, which involved all preparatory surgeries, but no pressure pulse was applied. Brains were processed for standard transmission electron microscopy, and stereological sampling conducted on genu, mid-callosal, and splenium regions. Because our primary objective was to monitor changes in surviving axons, the measurement variables were density and caliber (fiber cross-sectional area) of axons which met an operational definition of "intact." Specifically, axons were counted which met three criteria: (1) the membrane exhibited a continuous profile, (2) axoplasm contained at least one microtubule, and (3) axoplasm showed no degenerative debris. The sampling scheme, and an example of the unbiased counting frame, are shown in Fig. 15.3. This process yielded a total of 17,075 axonal profiles (6,659 from sham injured rats, and 10,416 from FPI rats), which were digitally traced and cross-sectional areas computed. Broken down by fiber type, 13,797 unmyelinated, and 3,278 myelinated, axons were measured. We predicted that axon caliber and density in our sham injured rats would be equivalent to that in naïve rats, because the sham procedure dissected only the midline scalp and cranium, without disturbing underlying tissue. Indeed, frequency distributions based on the 6,659 axons measured from our sham animals (Fig. 15.4a) demonstrated a close agreement with previous rodent studies (Waxman and Swadlow

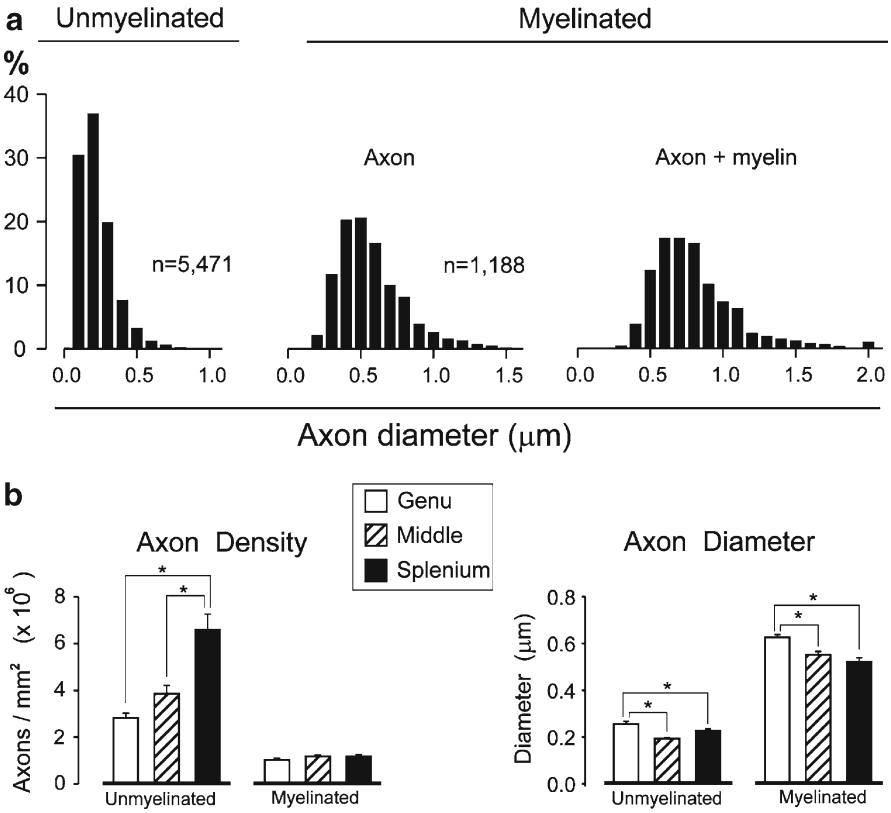

Fig. 15.4 Characterization of axon populations in sham lesion control rats. (**a**) Distributions of axon diameters for myelinated and unmyelinated axons. (**b**) (*left panel*) Separate analyses at CC regions revealed a rostral-to-caudal (genu-to-splenium) increase in the density of unmyelinated axons, but no gradient for myelinated axons. (*right panel*) Mean axon diameter was significantly greater in the genu than in either posterior region. *$p<0.05$. From Reeves et al. 2012, with permission

1976; Sturrock 1980; Gravel et al. 1990), the mean diameter of unmyelinated axons being 0.223 ± 0.002 μm, and myelinated 0.568 ± 0.006 μm. It was also notable that the sham material showed fiber caliber and density to differ significantly among the callosal regions. Unmyelinated axons exhibited a striking rostrocaudal gradient, being most numerous in the splenium (mean $= 6.2 \times 10^6/\text{mm}^2$) and falling off by 38.7 % in the mid-callosum, and by 54.8 % in the genu (Fig. 15.4b). In contrast, myelinated axon density in the various callosal regions did not differ from an overall mean of $1.1 \times 10^6/\text{mm}^2$. Axon diameters in sham rats also showed significant spatial variation, with genu fibers being largest for both unmyelinated (mean = 0.26 μm), and myelinated (mean = 0.63 μm) axon populations. At more caudal locations, mean diameter decreased for both fiber types (Fig. 15.4b).

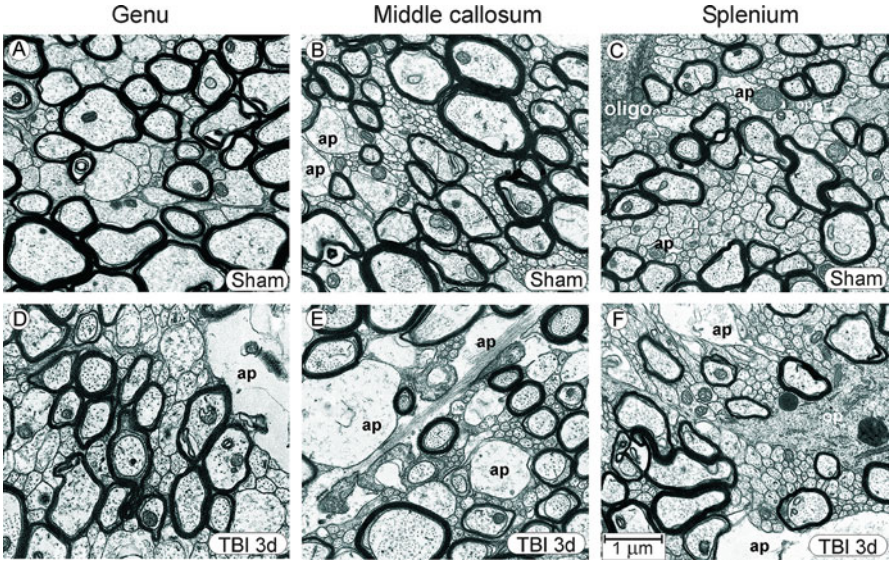

Fig. 15.5 Representative micrographs, showing genu, mid-callosum, and splenium regions in sham injured control rats (*top row*) and during the postinjury period when FPI-induced change in the unmyelinated axons was well developed (3 days postinjury) (*bottom row*). Even though quantitative analyses revealed significant morphometric changes to axonal dimensions at 3 days postinjury, the general architecture of injured tissue was similar to sham control tissue, although in some injured rats astrocyte processes were larger and encountered more frequently. *ap* astrocyte process, *oligo* oligodendrocyte cell body, *op* oligodendrocyte process. From Reeves et al. 2012, with permission

Representative micrographs from each region of the callosum in sham injured rats are shown in the top row of Fig. 15.5.

The moderate midline FPI induced a diffuse injury. No contused areas were observed during dissection, and the ultrastructural appearance of injured CC was typically quite similar to sham material, except that most injured cases exhibited more astrocyte profiles, consistent with reactive astrogliosis. Representative micrographs, showing genu, mid-callosum, and splenium regions at 3 days postinjury, are shown in the bottom row of Fig. 15.5. The following quantitative analysis first summarizes postinjury changes to the whole CC (pooling results from genu, middle, and splenium), and then considers injury effects in the specific callosal regions.

Analyses of axonal cross-sectional area, revealed a transient injury-induced decrease in unmyelinated axon area, with this effect reaching significance at 3 days (20.0 % below sham levels) and 7 days (22.8 % below sham levels) following injury. However, by 15 days postinjury mean unmyelinated axon area was not different from sham-operated rats (Fig. 15.6a). For the myelinated axons, there was a suggestion of an initial postinjury swelling at 3 h and 1 day, but these increases did not reach significance (Fig. 15.6a). Overall, myelinated fiber caliber did not significantly differ from sham control levels at any postinjury time point. Areal measures

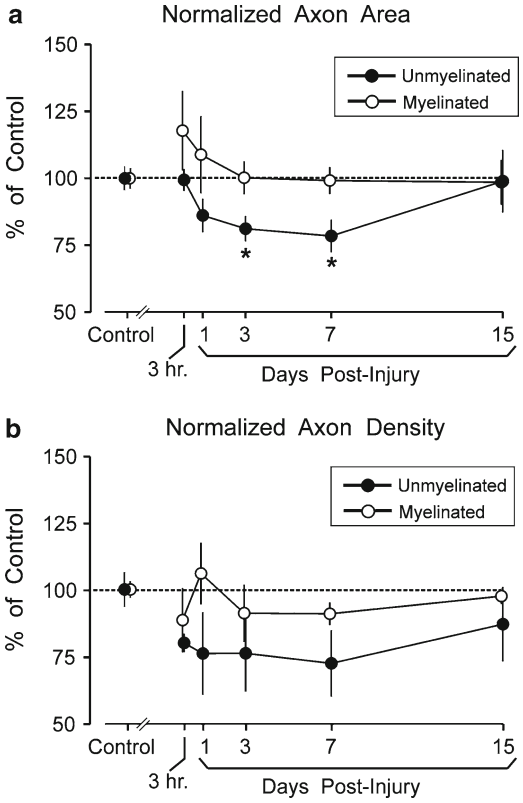

Fig. 15.6 Effect of FPI on cross-sectional area of axons and axon density. (**a**) Mean cross-sectional area of axons, averaged across all CC regions (genu, mid-callosum, splenium). Results are normalized to the mean axonal area measured in sham injured control rats. Time-dependent axonal shrinkage of unmyelinated fibers was significant at 3 and 7 days postinjury, but recovered to control levels by 15 days. FPI did not significantly alter cross-sectional areas of myelinated axons. (**b**) Mean normalized axon density, averaged across all CC regions. FPI effects on axonal density were more variable, and reductions in unmyelinated fiber density did not reach significance at any single survival interval. However, analyses which pooled together all postinjury time points (3 h to 15 days), providing a single injury group, indicated significant injury-related reductions in unmyelinated fiber density. FPI did not significantly alter density of myelinated axons. From Reeves et al. 2012, with permission

which included the axon plus myelin (contour "a" in Fig. 15.3) also did not significantly vary from sham levels at any time. These data allowed an evaluation of whether FPI altered the ratio of the inner axonal diameter to the total outer diameter (contours "c" to "a" in Fig. 15.3): the so-called g-ratio, which has been widely employed as a structural index of optimal axonal myelination since the historical work of Rushton (1951). Although the g-ratio has been reported to change in some

injury models (e.g., myelin thinning following spinal cord injury [Nashmi and Fehlings 2001]), the FPI did not induce a shift in this ratio from the sham mean of 0.708 ± 0.008, which approximates the optimal ratio for conduction velocity predicted by computer simulation (Smith and Koles 1970).

Compared to the substantial postinjury decline in mean diameter of unmyelinated axons, postinjury changes in the density of intact CC fibers were more variable. The mean density of CC unmyelinated axons was below the sham control level at all postinjury time points. However, this reduction did not reach significance in a statistical design with survival-interval as a factor, and which could detect time-dependent changes in density (Fig. 15.6b). However, analyses which pooled all postinjury time points together did indicate a significant injury-related reduction in unmyelinated fiber density ($F_{(1,28)} = 5.855$; $p = 0.022$). The density of myelinated axons was not significantly altered by the FPI (Fig. 15.6b). Ultrastructural analyses showed unmyelinated axons to exhibit abnormalities which were related to their decreased density, including membrane discontinuities or cytoplasmic abnormalities which prevented them from being scored as intact. This often took the form of atrophic changes where the axoplasm appeared to constrict, producing empty membranous folds and aberrant spaces in the adjacent extracellular compartment (examples in Fig. 15.7a). In other cases, degenerative changes affected clusters of unmyelinated axons, preventing their designation as intact. An additional pathological pattern, affecting unmyelinated fibers, was an apparent selective vulnerability of some relatively large axons, which often demonstrated axoplasmic constriction and membrane foldings. These malformed large axons were sometimes observed within fields of intact small unmyelinated axons, as illustrated in Fig. 15.7c. Although the unmyelinated axons, as a class, were more vulnerable to these injury conditions, these scattered instances of aberrant large unmyelinated fibers were exceptions to the general tendency for small diameter to comprise a risk factor after TBI.

Because diffusion tensor imaging in TBI patients commonly reveals a reduction in fractional anisotropy in the CC (reviewed by Maller et al. 2010), the finding of changes in axon morphology may have implications for the current theories of DAI. Following severe TBI, major white matter tracts, including the CC, have been reported to decrease axial, and increase radial, diffusivity (Arfanakis et al. 2002; Sidaros et al. 2008). These patterns of postinjury DTI alterations have been interpreted as consistent with Wallerian-like degeneration (Pierpaoli et al. 2001; Thomalla et al. 2004). However, the possibility that other axon pathologies may accompany degenerative changes, and further exacerbate the changes in diffusivity, have not previously been considered. It is conceivable that a reduction in unmyelinated axon caliber could also contribute to radial diffusion of water, and, in the context of clinical DAI, summate with Wallerian degeneration to produce the observed diffusivity alterations. Our observation, that the apparent shrinkage of unmyelinated axon diameters recovered to control levels over time, may be relevant to the fact that DTI abnormalities also improve in patients with good recovery. For example, diffusivity changes in the CC and internal capsule appeared to normalize by 1 year among patients with good outcome scores (Sidaros et al. 2008).

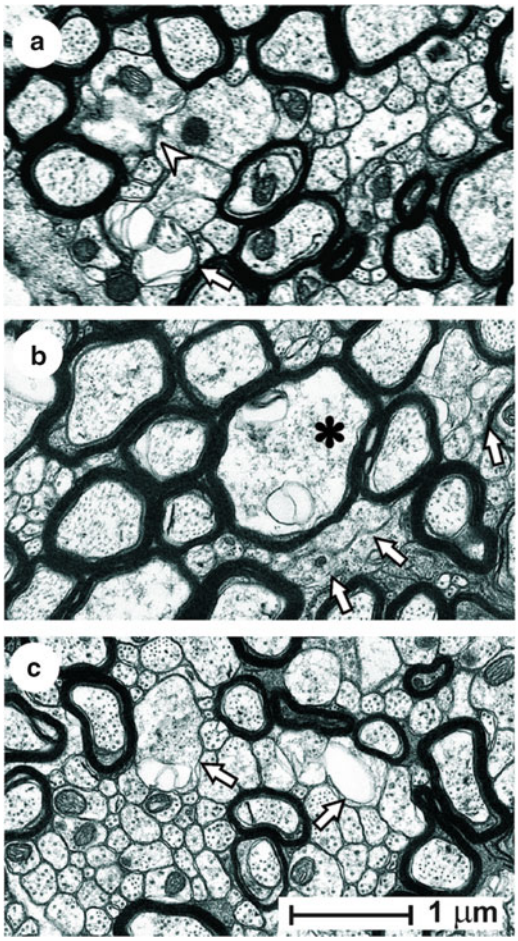

Fig. 15.7 Representative axonal profiles failing to meet the operational definition of intact, all from splenium at 3 days postinjury. (**a**) Isolated unmyelinated axons exhibiting membrane discontinuities (*arrowhead*) and membranous foldings apposed to aberrant extracellular spaces (*arrow*). (**b**) Clusters of unmyelinated fibers lacking distinct membranes (*arrows*), along with a myelinated axon (*asterisk*) with cytoplasmic abnormalities. (**c**) Example of vulnerability of relatively large unmyelinated axons (*arrows*) juxtaposed to intact small unmyelinated axons. From Reeves et al. 2012, with permission

Turning to a consideration of how injury effects varied along the rostro-caudal axis of the CC, our analyses of unmyelinated axons revealed a reduction in fiber caliber initially affecting the splenium at 1 day, and then progressing rostrally to impact the mid-callosal region at 3 days, and finally involving the genu at 7 days postinjury (Fig. 15.8 (*line graphs*)). The fact that changes to CC axons displayed a caudal-to-rostral temporal gradient may be related to heterogeneity in fiber composition along this axis. It has long been appreciated that the distributions of axon type and caliber are not continuous along the rostro-caudal axis in the CC of multiple species, from rodents to man (Gravel et al. 1990; Lamantia and Rakic 1990; Aboitiz et al. 1992, 2003). The high density of unmyelinated splenial axons, with decreasing numbers rostrally, was also confirmed in the present results, and these data are

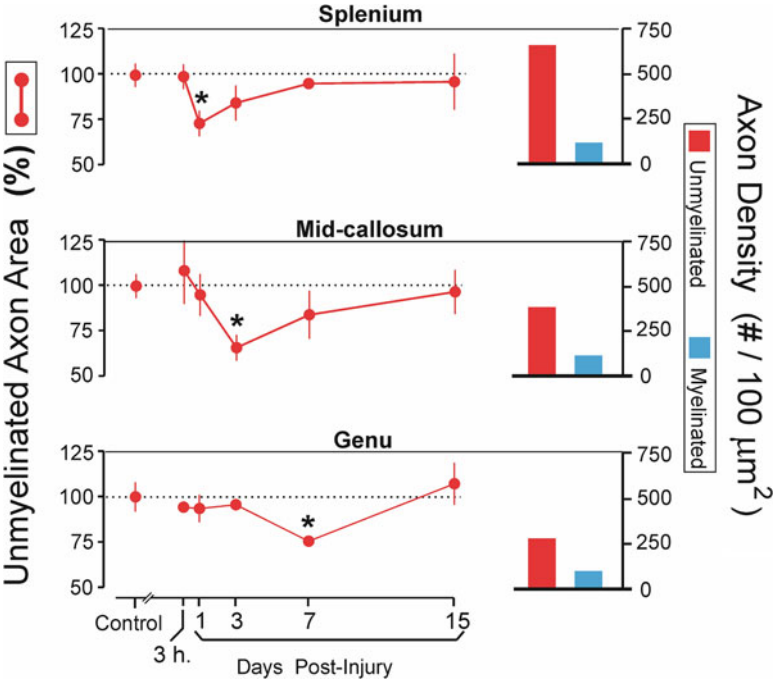

Fig. 15.8 Relationship between unmyelinated axon shrinkage in CC subregions and local density of unmyelinated axons. Effect of FPI on cross-sectional area of unmyelinated axons in the splenium, middle, and genu regions of the CC, normalized to sham levels (*line graphs*). FPI produced a caudal-to-rostral sequence of significant axonal shrinkage expressed at 1 day in the splenium, 3 days in the mid-callosum, and 7 days in the genu. Each region showed a recovery to sham control levels following the shrinkage. The temporal sequence of regional changes may be related to local density of unmyelinated axons (*histograms*). Line graphs from Reeves et al. 2012, with permission

reorganized into the histograms of Fig. 15.8. Juxtaposed to the splenium-to-genu temporal progression of TBI-induced reductions in axon caliber, the variation in unmyelinated axon density (Fig. 15.8 histograms) suggests the local proportion of these fibers may influence the onset of postinjury morphological changes. Large concentrations of unmyelinated fibers may, in itself, constitute a risk factor. Our laboratory is currently conducting electrophysiological recordings at the various CC regions, to assess the interaction of intrinsic fiber composition and post-TBI functional deficits. An additional motivation to evaluate injury effects, at CC subregions, is a number of clinical neuroimaging reports showing evidence for local differences in trauma vulnerability within the CC (Gentry et al. 1988; Rutgers et al. 2008; Matsukawa et al. 2011).

15.4 Electrophysiological Evidence for Differential Injury Responses in Unmyelinated and Myelinated Axons

15.4.1 The Compound Action Potential (CAP) as a Functional Assessment in Experimental TBI

Due to the diffuse nature of axonal damage in closed head injuries, the sparse distribution of injured axons may be difficult to detect even with modern imaging technology. As regards electrophysiological assessments in experimental animal TBI models, the diffuse pathology presents methodological challenges, especially approaches based on single unit recording or individual axons. A creative approach to this issue was reported by Andrew Baker and colleagues at the University of Toronto, who were the first to apply the technique of compound action potential (CAP) recording from CNS axons, as a functional assessment of axonal injury in experimental TBI. Because CAPs are a large amplitude field potential, representing the summation of individual action potentials in a population of axons, each CAP is already a sample of multiple axons. It is reasonable to assume that contributing to each CAP waveform are axons ranging from severely injured to uninjured, and thus CAP amplitude is a valid measure of TAI severity. Baker et al. (2002) reported that FPI in adult rats produced a significant suppression of CAPs evoked in the CC.

Our laboratory modified the methods of Baker et al. (2002) to enable separate quantification of CAPs generated by myelinated vs. unmyelinated axons. Using conventional brain slice recording technique, stimulating and recording electrodes were positioned into the CC of 450 μm thick coronal slices (Fig. 15.9a, b), at an inter-electrode distance of approximately 1.0 mm. With this electrode arrangement, each pulse evokes a waveform which is partially obscured by the stimulus artifact. However, we observed that lowering the temperature of the recording chamber slowed conduction sufficiently to allow a short-latency CAP waveform ("N1"), generated by fast-conducting myelinated axons, to be quantified separately from "N2," a CAP component generated by slower unmyelinated axons (Fig. 15.9c). It should be pointed out that there may be some minimal overlap of these distributions, i.e., a small number of especially large diameter unmyelinated axons may contribute to the early N1 CAP wave, and the smallest of the myelinated axons may be sufficiently slow conducting as to contribute to N2. However, work in multiple laboratories has converged on the conclusion that the clear majority of the distributions are nonoverlapping, and N1 and N2 are generated predominantly by myelinated and unmyelinated axons, respectfully. First, diameters of the ultrastructurally observed populations of myelinated and unmyelinated callosal fibers agree well with recorded conduction velocities. Specifically, Waxman and Swadlow (1976) noted that the diameters of myelinated (0.3–1.85 μm in diameter) and unmyelinated (0.08–0.6 μm) fibers, which they measured in the posterior callosum, corresponded well with the distribution of observed conduction velocities (0.3–12.9 m/s). Those same authors interpreted refractoriness and threshold results to suggest that the N1 and N2 field

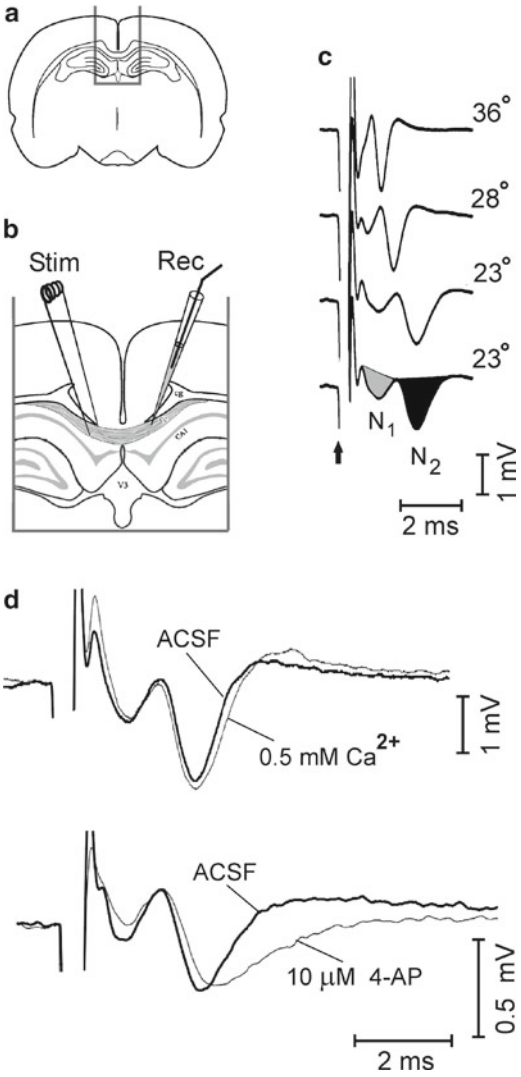

Fig. 15.9 Placement of electrodes for callosal CAP recording, and responses of N1 and N2 CAP components to temperature and ionic manipulations. (**a**, **b**) Stimulating and recording electrodes were positioned in midline CC separated by approximately 1.0 mm. (**c**) Decreasing bath temperature slowed conduction time, enabling quantification of N1 (*gray shading*) and N2 (*black shading*) waveforms. (**d**) Recording in low $[Ca2^{+}]_{o}$ did not significantly alter evoked CAPs, while bath application of the K^{+} channel blocker (4-AP) selectively prolonged the N2 CAP component. From Reeves et al. 2005, with permission

components were produced by fibers that did not vary simply along a single continuous dimension, but more likely by the presence or absence of myelin. Our laboratory observed that externally applied potassium channel blocker (4-AP) prolonged only the N2 CAP component, leaving N1 unchanged (Fig. 15.9d). This is consistent with an N2 generated by unmyelinated axons, having 4-AP-sensitive K^{+} channels along the entire axolemma, whereas in myelinated axons the channels are located along the internodal axolemma, beneath the myelin sheath and "masked" from externally applied 4-AP. These results are in agreement with earlier work in dorsal column axons (Kocsis and Waxman 1980) as well as CC (Swanson et al. 1998).

Figure 15.9d also shows that recording CAPs after lowering the perfusate to a low-calcium condition (0.5 mM) did not alter the waveform from that seen in normal artificial cerebrospinal fluid (ACSF), consistent with the expectation that callosal CAPs are a purely axonal phenomena, and do not reflect any synaptic events.

15.4.2 Unmyelinated and Myelinated Axons Exhibit Differential Conduction Deficits After TBI

Analysis of CAPs following FPI revealed that the myelinated and unmyelinated waveform components were differentially affected by the injury, and showed different courses of postinjury recovery (Reeves et al. 2005). We routinely evaluate CAPs using an "input–output" function: a graduated series of stimulus intensities, ranging from near-threshold to maximum response. Figure 15.10a illustrates representative CAPs from input–output series (superimposed) from a sham control rat and from a rat recorded at 1 day post-TBI. Suppression of both N1 and N2 was typical at that survival period. The curves in Fig. 15.10b, c illustrate the mean injury-induced suppression of N1 and N2 amplitude, respectively, over the full range of stimulation current used. For both N1 and N2, this injury effect was greatest at 1 day postinjury. Statistical analyses indicated that the N1 amplitudes were significantly depressed at postinjury times 3 h, 1 day, and 3 days, but were no longer significantly different from control levels at 7 days postinjury. N2 amplitudes remained significantly below control levels at all postinjury survival intervals (3 h to 7 days), and no significant time-dependent recovery was observed for N2 amplitudes.

Postinjury decreases in CAP amplitude, such as those noted here, may result from fewer axons recruited into the CAP waveform; for example, due to dead axons, or inactivation of axons through a depolarization block. Alternatively, the injury process may not alter the number of responsive fibers, but instead alter conduction properties and reduce amplitudes of action potentials in individual axons, which would also reduce the amplitude of the overall CAP signal. Thus, amplitude measures of the CAP waveform, alone, cannot distinguish between these alternative pathological processes. This issue may be addressed using stimulation protocols which assess the intrinsic functional properties of individual axons, and are less sensitive to the absolute numbers of recruited fibers. For example, refractoriness of callosal fibers may be analyzed by quantifying the suppression of the second CAP response in paired stimulus trials. Figure 15.11 shows example series of the second response evoked in paired stimulus presentations, at the indicated interpulse intervals (IPI, 1.5–6.0 ms), after subtracting out the responses to the conditioning pulse, for a control slice (Fig. 15.11a) and for a slice recorded at 1 day postinjury (Fig. 15.11b). Figure 15.11c plots the CAP amplitude elicited by the second pulse in each paired stimulation (C2) divided by the CAP amplitude to single pulse stimulation (C1). These C2/C1 ratios were averaged for each survival group and plotted for N1 and N2. Rightward shifts in these curves indicate increases in the refractory recovery cycle in the CC axons, consistent with axonal damage. For example, these

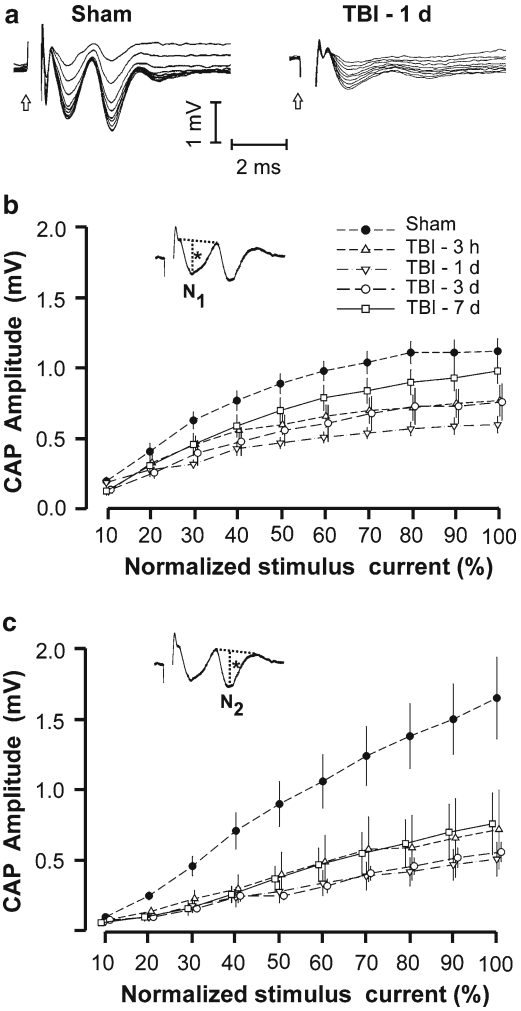

Fig. 15.10 Differential effects of TBI on N1 and N2 CAPs. (**a**) Recruitment of field potential with graduated series of stimulus pulses (10–100 % of maximum) for a sham control rat and for a rat recorded at 1 day postinjury. (**b**) Average amplitude of N1 over the full range of stimulation current used, for sham and TBI groups. N1 amplitude was significantly decreased by TBI at 3 h, 1 day, and 3 days, but was not at 7 days. (**c**) Average amplitude of N2 over the full stimulus range, for sham and TBI groups. More persistent injury-induced suppression of average response amplitude was observed for the N2, which remained significantly below control levels at all postinjury survival intervals (3 h, 1 day, 3 days, and 7 days). Inserts in panels (**b**) and (**c**) show CAP amplitude measurement technique for N1 and N2 components (height of vertical line *asterisk*). From Reeves et al. 2005, with permission

curves show the sham N1 waveform, evoked by the second of a pair of pulses, achieved 50 % of the amplitude of a single pulse presentation, when the interpulse interval was approximately 3.7 ms, and this parameter for the N2 field component was 4.5 ms. Averaged over all postinjury groups, the fluid percussion injury degraded the refractory performance for these fibers by approximately 0.5 ms for both N1 and N2 field components. The refractory curves were significantly right-shifted at 3 h, 1 day, and 3 days, for N1, and at 3 h and 1 day for N2. The refractory curves showed evidence of recovery (left-shifts), and by 7 days were not statistically different from control curves for either the N1 or N2 wave component.

The refractoriness results suggested that postinjury CAPs reflected, at least in part, injury-induced alterations in the functional properties of individual axons, such

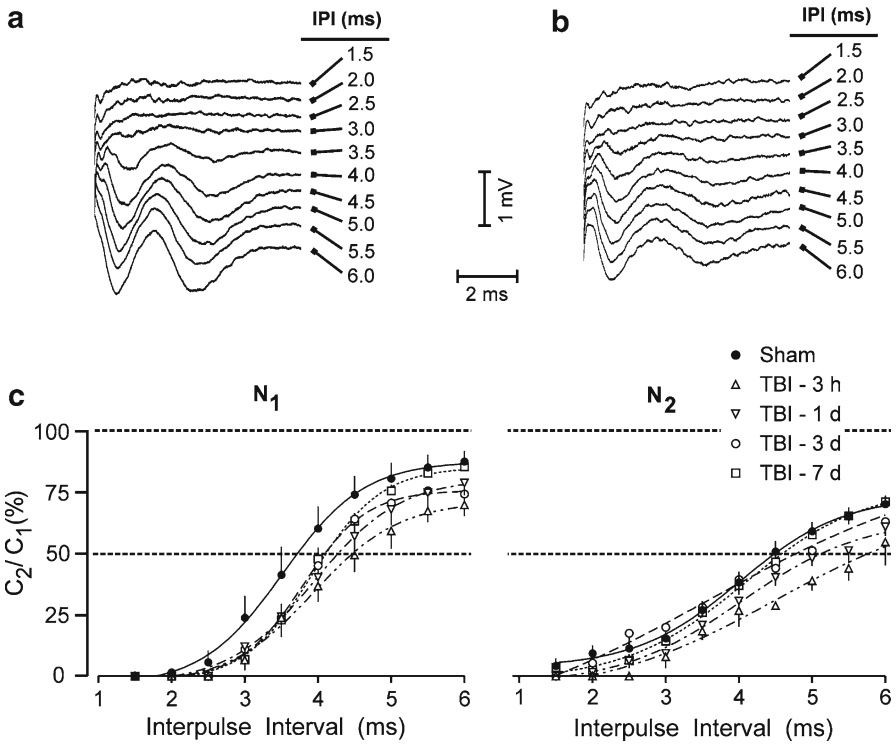

Fig. 15.11 Effect of TBI on callosal CAP refractoriness. Examples waveforms at top show second potentials in paired responses, after subtraction of response to the conditioning pulse, from a sham control rat (**a**) and from a rat recorded at 1 day post-TBI (**b**), at indicated interpulse intervals from 1.5 to 6.0 ms. (**c**) Plots of mean CAP amplitude elicited by the second pulse in each paired stimulation (C2) divided by the CAP amplitude to single pulse stimulation (C1), for control and injured groups. Average C2/C1 ratios were fitted to Boltzmann sigmoid curves, and showed significant increases in refractoriness (*rightward curve shifts*) at 3 h, 1 day, and 3 days for N1 (*left panel*) and at 3 h and 1 day N2 (*right panel*). From Reeves et al. 2005, with permission

as level of depolarization or pathological changes to Na^+ channels. Refractoriness has long been recognized to depend largely on recovery of Na^+ channels from inactivation (Hodgkin and Huxley 1952), and is sensitive to changes in membrane potential (Burke et al. 1998). A depolarizing shift will increase the extent of Na^+ channel inactivation. The observed refractory deficits are consistent with injury-induced axonal depolarization or alterations in the function of Na^+ channels: changes which may not be lethal but recover over time. A tetrodotoxin (TTX)-sensitive Na^+ influx has been reported as an initiating pathology in axonal injury, and was associated with proteolytic damage to Na^+ channel α-subunits (Iwata et al. 2004). The primary ionic event, generating the callosal CAP, is influx through voltage gated Na^+ channels, and TTX has been reported to entirely suppress callosal CAPs in brain slices (Swanson et al. 1998).

It is useful to compare the CAP recording results with the preceding ultrastructural analyses. In this regard, the most robust ultrastructural finding was a time-dependent reduction in the average diameter (cross-sectional area) of unmyelinated CC axons, which had recovered to control levels by 15 days postinjury. While the ultrastructural results also indicated a post-TBI reduction in the number of unmyelinated axonal profiles which could be categorized as "intact," this experimental effect was more variable than caliber changes, but also appeared to recover by 15 days. Our study of post-TBI CAP suppression, which examined survival periods up to 7 days, was conducted prior to the finding of ultrastructural recovery at 15 days. This, of course, is an interpretive limitation of this CAP dataset. However, it is notable that the FPI affected the unmyelinated axon population to a much greater extent than the myelinated fibers: both ultrastructurally and with regard to CAP amplitude. Moreover, the primary ultrastructural finding was a transient reduction in unmyelinated axon caliber, and not irreversible loss of axons. While we have not extended CAP recording to 15 days postinjury, to confirm a functional recovery in the unmyelinated population to match the ultrastructural results, certain electrophysiological findings were consistent with reversible changes in axons rather than with axon death. The refractoriness findings demonstrated a cycle of deficit and recovery. A similar interpretation was offered for analyses which assessed threshold and excitability properties using a "strength-duration" stimulus protocol [not illustrated here], which indicated a significant suppression of excitability at 3 h postinjury for both N1 and N2, with subsequent recovery (Reeves et al. 2005). The finding of posttraumatic structural changes preferentially affecting unmyelinated axons of the brain is novel, and quite dissimilar from the well characterized cytoskeletal breakdown and swellings noted in heavily myelinated brainstem tracts (Pettus et al. 1994; Povlishock 1992; Povlishock et al. 1997; Okonkwo et al. 1999; Buki et al. 1999, 2003; Singleton et al. 2001; Stone et al. 2001, 2002; Marmarou and Povlishock 2006). It must also be stressed that the pathological changes observed in the brainstem tracts were usually elicited with the impact acceleration injury model, and this involves injury forces greater than applied in the FPIs described here. However, we hypothesize that aberrant changes in the unmyelinated axon population, including the reduction in caliber, likely coexist with focal myelinated pathology in models of more severe TBI, at all levels of the neuraxis.

15.5 Unmyelinated and Myelinated Axons Exhibit Differential Responses to Neuroprotective Compounds

To date, no effective treatment for DAI has been demonstrated for head injured patients. However, studies using rodent models of TBI have demonstrated promising reductions in axonal injury using treatment with immunosuppressant drugs, especially FK506 and Cyclosporin-A (CsA). These compounds reduce axonal damage in multiple ways following TBI: attenuating cytoskeletal compaction (Buki et al. 1999; Okonkwo et al. 1999), and reducing impairments to axonal transport (Singleton et al. 2001; Marmarou and Povlishock 2006). Here, we discuss how

these compounds also benefit axonal conduction properties following FPI (Reeves et al. 2007; Colley et al. 2010). CsA and FK506 are widely used clinically to reduce activation of the immune system in organ transplantation, by inhibiting the enzyme calcineurin, resulting in decreased interleukin (IL-2) production and T lymphocyte activation. However, neuroprotective effects of CsA and FK506 do not depend on immunosuppression, and involve calcineurin pathways separate from interleukin production. For example, axonal neuroprotection may result when calcineurin is prevented from acting on known axonal substrates: MAP2, tubulin, and tau protein (Goto et al. 1985), and neurofilament proteins (Eyer and Leterrier 1988).

15.5.1 Preinjury Administration of FK506

As a first approach to evaluating the neuroprotective efficacy of FK506 in alleviating TBI-induced impairments in the function of CC axons, we selected a preinjury treatment paradigm: administering FK506 at 30 min prior to FPI. This strategy was not intended to have a direct clinical relevance; for obvious reasons, in any practical application a drug cannot be administered prior to an injury. Instead, our objective was to examine the protective potential of the compound, where conditions are optimal to detect treatment effects on the earliest injury phases, including primary axonal damage occurring during the mechanical trauma. This was the first study (Reeves et al. 2007) to address the specific issue of differential therapeutic efficacy in unmyelinated and myelinated axons, in response to a neuroprotectant administration.

The study methodology, in brief, was to administer 3 mg/kg FK506 intravenously at 30 min prior to FPI in adult rats, using injury parameters identical to the above ultrastructural and electrophysiological experiments. Previous work had demonstrated that this intravenous dosage crosses the blood–brain barrier and establishes therapeutic levels of brain parenchymal concentration (Singleton et al. 2001) which correlate with near maximum inhibition of calcineurin (Ochiai et al. 1989; Butcher et al. 1997) consistent with neuroprotection. CAP recording was conducted in vitro, as described above, at 24 h following the FPI. A subset of rats were used to evaluate FK506 efficacy in reducing the prevalence of amyloid precursor protein (APP)-labeled axons, which is a commonly used marker for impaired axonal transport (Stone et al. 2000).

Consistent with our earlier study, FPI suppressed callosal CAP amplitudes when measured at 24 h postinjury. Representative CAP waveforms, evoked using graduated stimulus levels in input–output testing, are shown in Fig. 15.12a for vehicle- and FK506-treated sham and injured rats. CAPs from a vehicle-treated sham and TBI rat (left side of Fig. 15.12a) are representative of the profound response reductions observed postinjury. Mean CAP amplitudes are plotted for each analytic group in Fig. 15.12b, as curves relating evoked CAP amplitude to normalized stimulus current. Statistical analysis of these curves showed that TBI significantly suppressed both myelinated (N1) and unmyelinated (N2) CAP components.

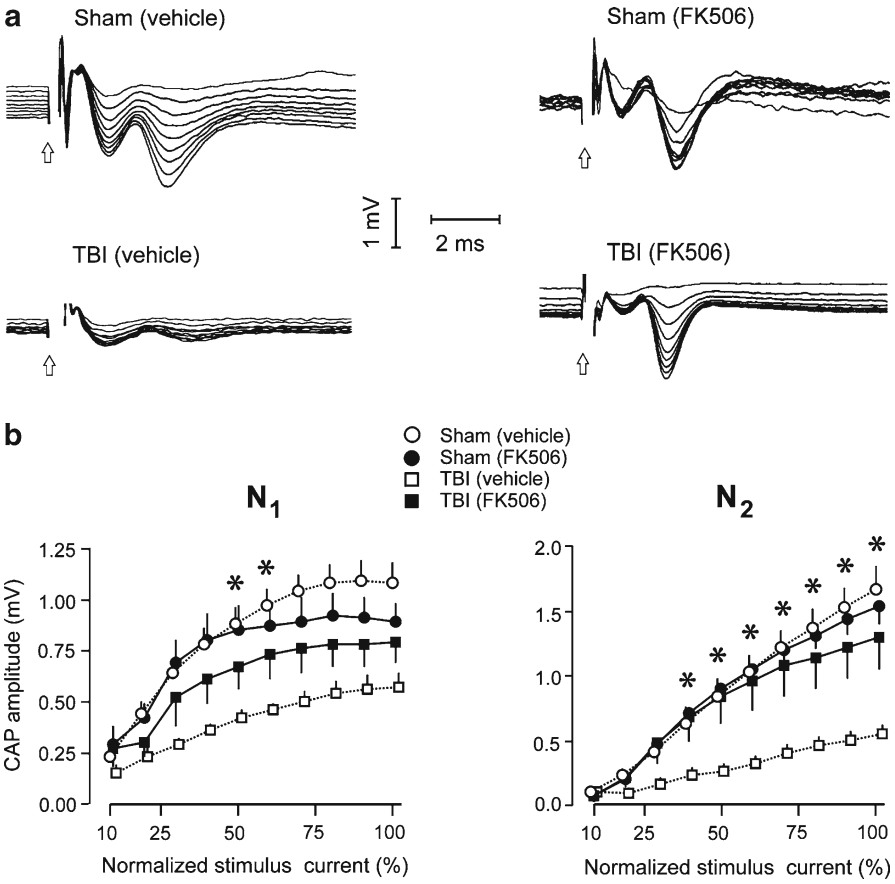

Fig. 15.12 Differential effects of FK506 treatment on postinjury suppression of callosal N1 and N2 CAP amplitudes. (**a**) Samples of CAP field potentials generated in input–output testing. (**b**) (*Left panel*) Average amplitude of N1 over the full range of stimulation current used, for all groups. N1 amplitude was significantly decreased by TBI, but FK506 treatment provided significant neuroprotection only at selective stimulus intensities (50–60 % of maximum). (*Right panel*) Average amplitude of N2 over the full stimulus range, for all groups. TBI produced a more severe suppression of the N2 CAP amplitude, at a greater range of stimulus intensities (40–100 %). From Reeves et al. 2007, with permission

The FK506 pretreatment produced a marked protection against postinjury decreases in unmyelinated CAP amplitude, and a more moderate level of protection for myelinated amplitudes. FK506 effects were dependent on the level of stimulus current, and the drug effects were evaluated at specific levels of normalized stimulus intensity. N2 CAP amplitudes recorded in FK506-treated TBI rats were significantly elevated above those in vehicle-treated TBI rats. Comparisons at specific levels of stimulus intensity showed the FK506 protection of the N2 CAPs to be significant at stimulus levels of 40–100 % (asterisks in Fig. 15.12b). In contrast,

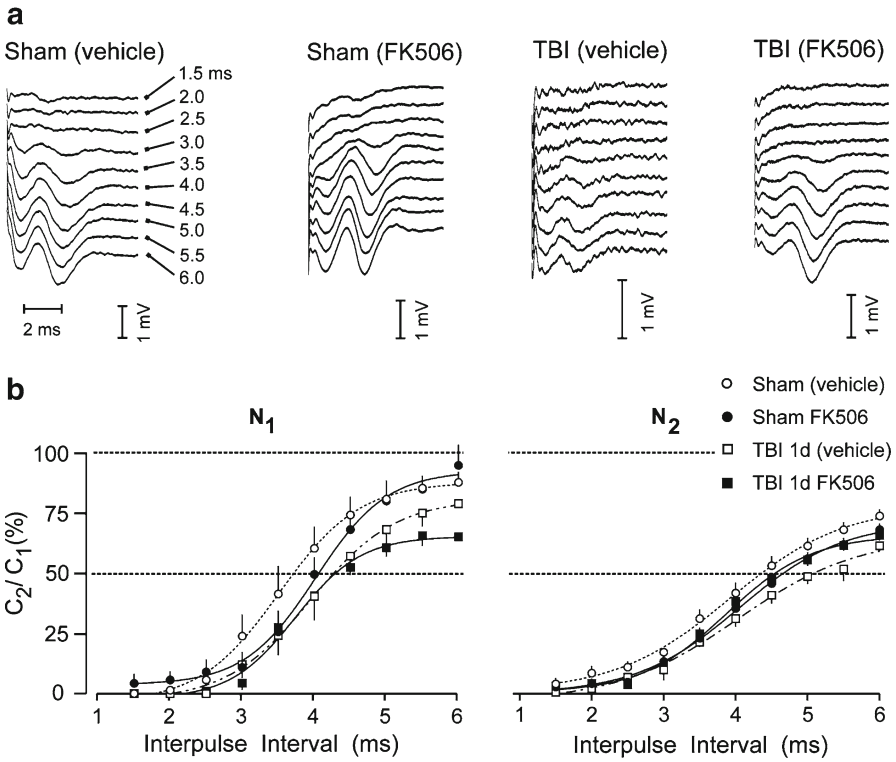

Fig. 15.13 Effect of TBI and FK506 treatment on callosal CAP refractoriness. (**a**) Example waveforms show second potentials in paired responses (interpulse intervals = 1.5–6.0 ms), after subtraction of response to the conditioning pulse, of representative cases from each experimental group. (**b**) Plots of mean CAP amplitude elicited by the second pulse in each paired stimulation (C2) divided by the CAP amplitude to single pulse stimulation (C1), for all groups. Average C2/C1 ratios were fitted to Boltzmann sigmoid curves, and showed TBI-induced increases in refractoriness (*rightward curve shifts*) which was significant for N1 and N2. FK506 prevented this injury effect only for the N2 CAP component. From Reeves et al. 2007, with permission

FK506 treatment led to significant N1 CAP protection only at two stimulus intensities (50 and 60 %). These results, and additional statistical analyses contained in Reeves et al. (2007) were consistent with a larger degree of FK506 protection for unmyelinated axons than for myelinated axons.

Refractoriness of the callosal fibers was analyzed, using methods described above, in the evaluation of FK506 neuroprotection. Figure 15.13a shows representative series of the second response evoked in paired stimulus presentations, at the indicated interpulse intervals (IPI, 1.5–6.0 ms), and Fig. 15.13b plots CAP amplitudes elicited by the second pulse in each paired stimulation (C2) divided by the CAP amplitude to single pulse stimulation (C1). Refractory results showed that FPI produced significant rightward shifts for both N1 and N2. However, FK506 treatment significantly ameliorated this deficit only for the N2 CAP, the refractory curve for which was not different from that of vehicle-treated sham rats. In TBI rats treated with FK506 the refractory curve

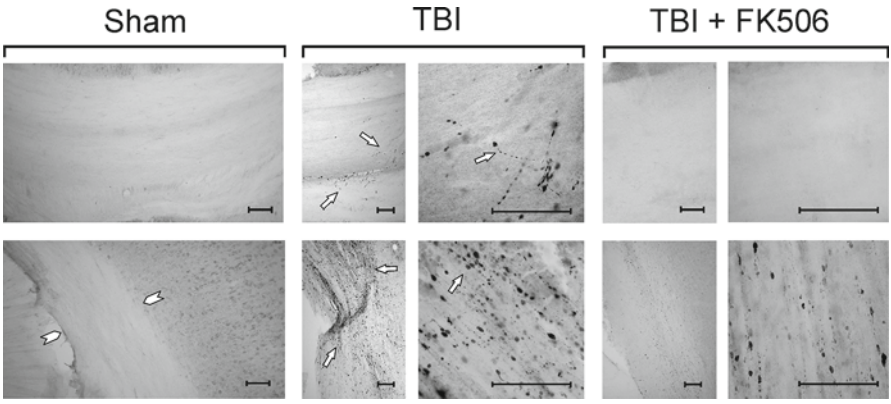

Fig. 15.14 FK506 effects on postinjury increases in APP labeled axons within the CC and subcortical white matter adjacent to electrophysiological recording at 24 h postinjury. *Top row*: Representative sections show immunohistochemical detection of APP labeled damaged axons in mid-dorsal corpus callosum of sham-injured, vehicle- and FK506-treated TBI conditions. As previously observed, APP staining of injured axons was absent in the sham control CC, but visible at discrete foci after TBI (*arrows*). With FK506 treatment APP profile was similar to that of sham control. *Bottom row*: Representative sections show APP label in subcortical white matter of sham-injured, vehicle- and FK506-treated TBI conditions. As in CC, sham control cases showed no APP staining of white matter axons (*arrowheads*). After TBI, significant axonal damage is detected with APP in the white matter (*arrows*). FK506 treatment reduced APP staining. Calibration bars = 50 μm. From Reeves et al. 2007, with permission

for the N1 CAP remained significantly right-shifted relative to vehicle-treated sham rats. While the absolute magnitudes of these injury-induced rightward shifts were modest (0.55 ms for N1 and 0.73 ms for N2), the significance of the curve shifts suggested that TBI altered fundamental activation properties of the axons, slowing the recovery cycle times of both the myelinated and unmyelinated axon populations. FK506 treatment reduced refractory changes only for the N2 CAP, consistent with a differential therapeutic effect for the unmyelinated axon population.

In the histological component of the study, APP immunoreactive swellings were observed in the CC and adjacent subcortical white matter at 24 h postinjury (Fig. 15.14). Qualitative comparisons between the FK506-treated and vehicle groups revealed consistent and striking differences. FK506-treated animals showed dramatic reduction of immunoreactive axonal swellings in all regions sampled, although these immunocytochemical observations could not discriminate between unmyelinated and myelinated damage.

15.5.2 Postinjury Administration of Cyclosporin-A

In a subsequent study (Colley et al. 2010) we further pursued the issue of neuroprotection of immunophilin ligands, but now investigating CsA using a more clinically relevant postinjury administration paradigm. While FK506 neuroprotection is

attributed to calcineurin inhibition, recent evidence indicates that CsA protects against TBI primarily by preventing mitochondrial permeability transition pore (MPTP) formation. The CsA derivative NIM811, which inhibits MPTP formation but not calcineurin activity, was reported to retain the same neuroprotective potency as CsA in reducing injury-induced spectrin proteolysis, axonal degeneration, and neurologic dysfunction (Mbye et al. 2008, 2009).

In the CsA study, methods for injury production and electrophysiological assessments were identical to those of the FK506 study above. Rats received a single 20 mg/Kg bolus of CsA, or cremaphor vehicle, at either 15 m or 1 h following a moderate midline fluid percussion injury. Figure 15.15 summarizes effects of injury and CsA treatment on CAP amplitude. In our assessments of CsA efficacy, we reported on CAP area as the primary dependent variable, although it is important to note that we obtain essentially identical results using either waveform peak or area-under-the-curve as endpoints. Figure 15.15b shows CAPs collected at maximum stimulus intensities, representative of vehicle-treated sham and TBI rats, as well as TBI rats given CsA at 15 m and 1 h postinjury. These sample CAPs typify the injury-induced suppression observed in both N1 and N2 CAPs (compare Sham + veh and TBI + veh waveforms), and the attenuation of this deficit in rats administered CsA at 15 m postinjury (compare TBI + veh and TBI + CsA (15 m) waveforms).

Input–output curves, averaged for each experimental group, are shown in Fig. 15.15c. Assessing the effects of injury in this way, across the full input–output range, revealed a greater injury deficit, and a larger degree of CsA neuroprotection, for the myelinated than for the unmyelinated CAPs. In TBI rats treated with CsA at 15 min postinjury the myelinated CAP amplitude was no longer suppressed below the Sham + veh level, and was significantly elevated above the TBI + veh group, indicating a significant neuroprotection for the myelinated fibers. Delaying CsA treatment until 1 h postinjury entirely eliminated the neuroprotection for the N1 CAP area.

In contrast to the significant injury and drug effects seen for the myelinated CAP amplitude, the input–output curve measurements for the unmyelinated CAP did not reveal significant injury or treatment effects (right panel in Fig. 15.15c). However, inspection of the N2 input–output curves suggested that the TBI + CsA (15 m) group tended to elevate above the TBI + veh group as stimulus intensity was increased. Thus, it is possible that the detection of a statistically significant degree of CsA neuroprotection, in the case of the N2 CAP, may depend in part on stimulus conditions. One factor underlying dissimilar N1 and N2 area results may be a difference in how myelinated and unmyelinated axons are recruited into the CAP response as stimulus current is increased from threshold to higher levels. To address this issue, the effects of injury and CsA treatment were also examined at a static level of stimulus intensity. Figure 15.16 shows mean CAP amplitude measured at the maximum current level used during input–output testing (100 % level in Fig. 15.15c). This approach continued to show a neuroprotection afforded to the myelinated axons when CsA was delivered at 15 m postinjury, as indicated by the fact that N1 amplitude in TBI + veh rats fell below sham levels, while N1 amplitude in TBI + CsA(15 m) rats was not different from sham cases. Importantly, this analysis also revealed a significant increase in N2 CAPs in TBI rats administered CsA at 15 m after injury, which may reflect a beneficial effect of CsA, although the TBI + vehicle group

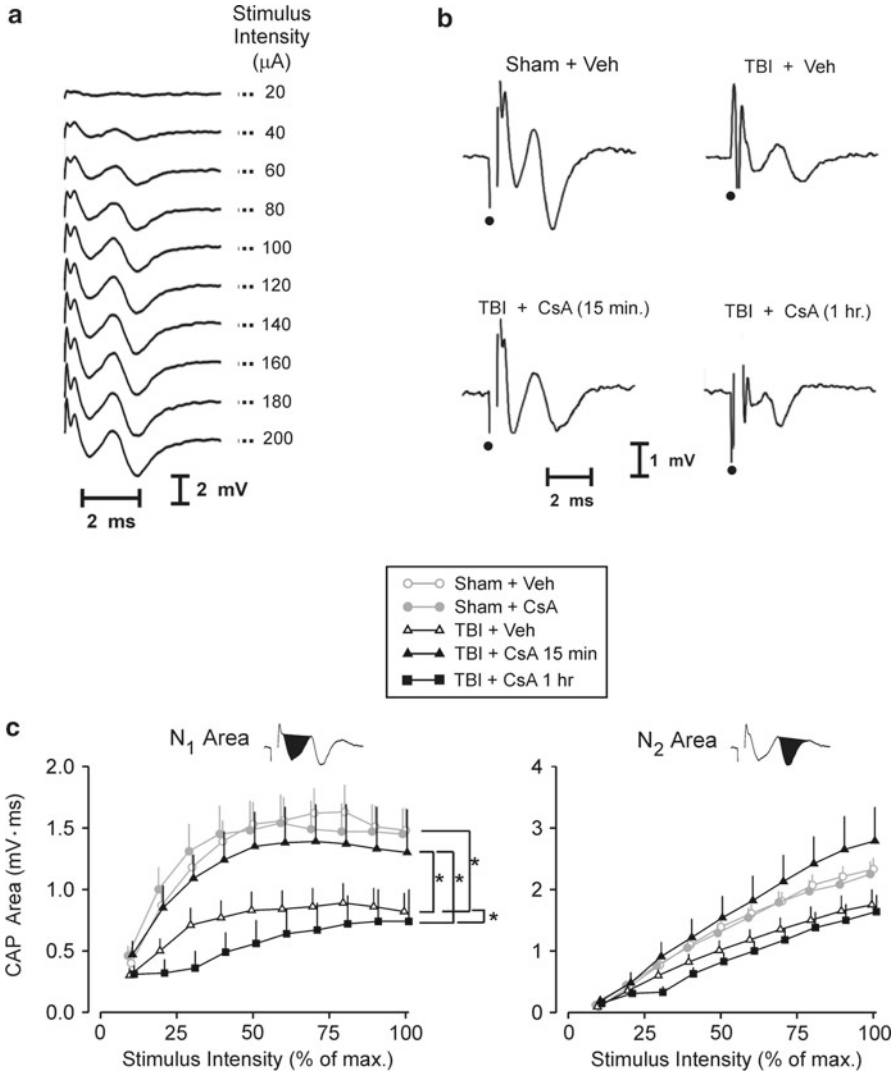

Fig. 15.15 Effects of injury and CsA treatment on CAP area. (**a**) Input–output series evoked with stimulus currents ranging from threshold to CAP maximum. (**b**) Representative CAPs evoked at the maximum stimulus level for vehicle treated sham and TBI rats, and for TBI rats given CsA at 15 m and 1 h. (**c**) Input–output curves, showing N1 and N2 CAP area plotted as a function of normalized stimulus intensity. The average input–output function of the N1 CAP area was protected in TBI rats by treatment with CsA at 15 m, but not at 1 h, postinjury. Average N2 area input–output functions were not significantly shifted by injury or CsA treatment. From Colley et al. 2010, with permission

narrowly failed to show a statistically significant injury effect. This instance of a mild injury effect to unmyelinated CAPs contrasted with patterns of injury observed previously (Ai et al. 2007; Reeves et al. 2005), where unmyelinated deficits were equal to, or greater than, those in the myelinated axons. We attributed this to a

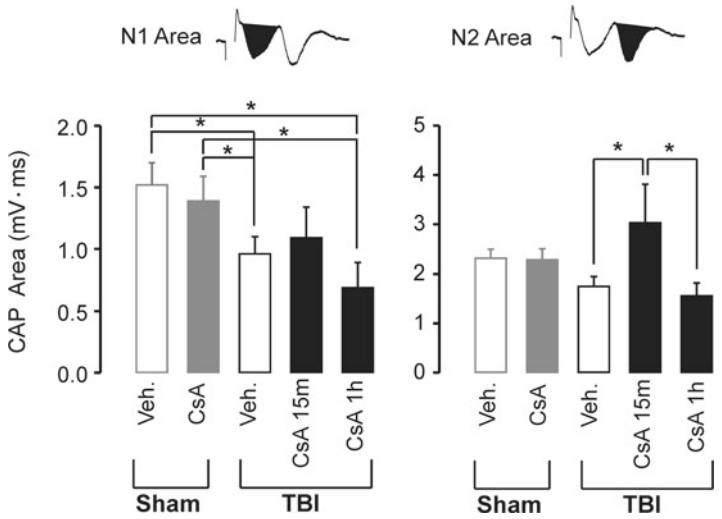

Fig. 15.16 Effects of injury and CsA on area of CAPs evoked with maximum stimulation. Mean N1 and N2 areas, evoked using the 100 % stimulation intensity, are plotted for each analytic group. N1 areas in TBI + veh rats were significantly suppressed below sham levels, but N1 areas in TBI + CsA (15 m) rats were not different from those of sham rats. For the N2 CAP areas evoked with maximum stimuli, there was not a significant injury effect (Sham + veh vs. TBI + veh), but CsA treatment administered at 15 m post-TBI significantly elevated the N2 area above vehicle-treated rats. This drug effect was not present when CsA was given at 1 h postinjury. From Colley et al. 2010, with permission

neuroprotective effect reported for the cremaphor vehicle (Setkowicz and Guzik 2007), and used in the present study. It is possible that the cremaphor-based vehicle exerted a protection selective to the unmyelinated axons, underlying the mild injury and drug effects observed for these fibers. Related to this issue, some aspects of the CsA evaluation also suggested modest detrimental effects when CsA was administered at 1 h postinjury. For example, the myelinated input–output function of the TBI + CsA (1 h) group was shifted below that of the TBI + veh group. This result, along with abnormalities affecting CAP durations and refractoriness, suggested CsA action led to fewer fibers being recruited into the aggregate CAP response (see detailed analyses in Colley et al. 2010). However, it was concluded that the CsA treatment conferred an overall protective effect, providing a benefit to CAP amplitude and improved high-frequency responding in myelinated axons when CsA was administered at 15 min postinjury (Fig. 15.17).

Although the analyses of CsA neuroprotection revealed a complex set of experimental effects, it was clear that the postinjury administration of the drug conferred greater benefit to the myelinated than to the unmyelinated axon population. Our laboratory has completed parallel experiments, not yet submitted for publication, evaluating the postinjury administration of FK506, which also showed a disproportionate benefit for myelinated axons. Our overall findings regarding functional neuroprotection with immunophilin ligands, to date, continue to underscore how very differently the unmyelinated fiber population responds to TBI, and evidently to this

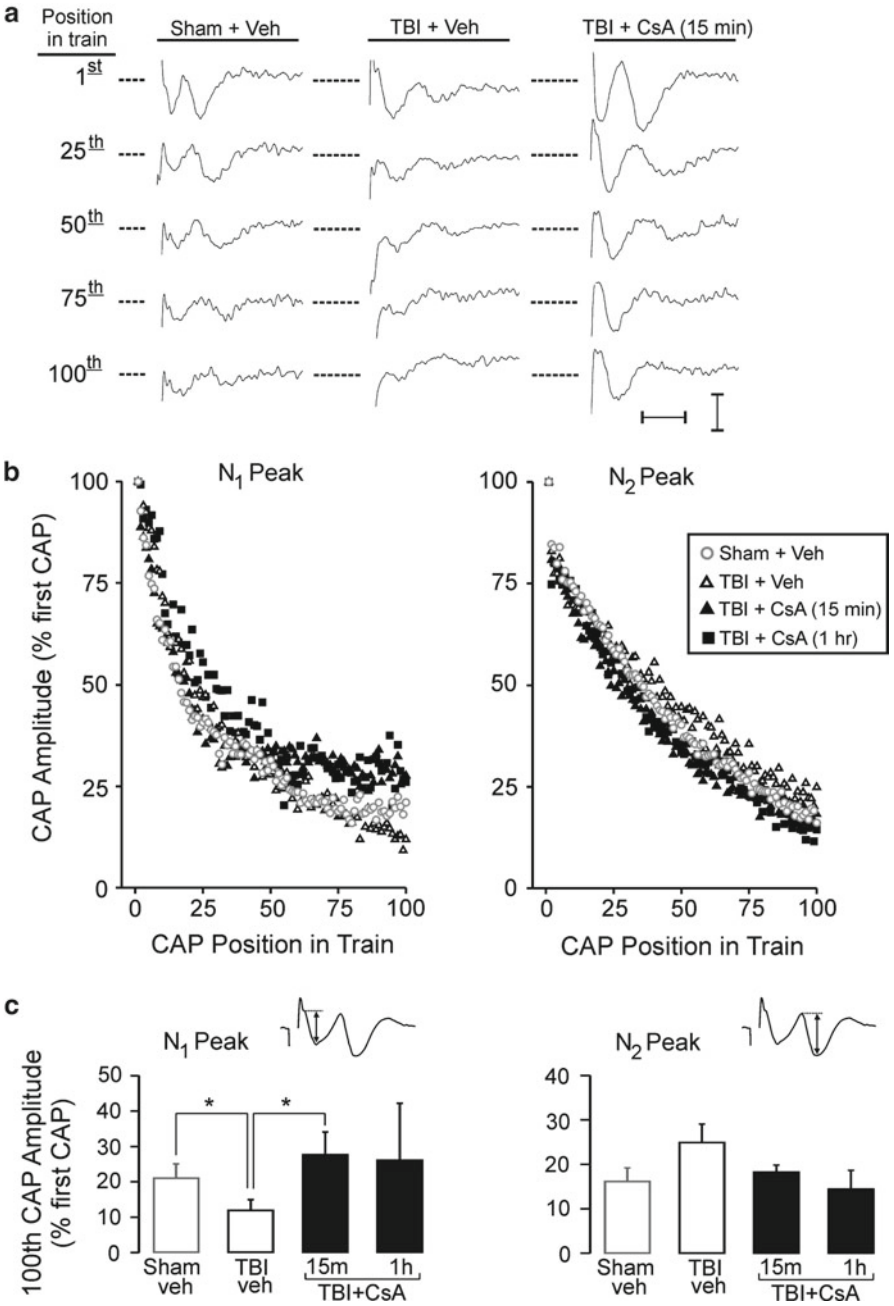

Fig. 15.17 Effects of injury and CsA treatment on high frequency responding. (**a**) Example evoked CAPs (single, nonaveraged) at serial position 1, 25, 50, 75, and 100 in response to a 100 Hz stimulus train of 1 s duration. Calibration: 1 mV×2 ms. (**b**) Scatterplot showing mean of CAP peaks for each 100 responses in high frequency train, with each data point normalized to the first CAP in the series. In N1 scatterplot, note fatigue of TBI+veh responses and preservation of CsA-treated responses between CAP position 75–100. (**c**) Group analysis of the N1 CAP number 100, expressed as a percentage of CAP number 1, showed TBI+veh condition to be significantly depressed by the injury, but CsA treatment at 15 m provided significant protection of this function. From Colley et al. 2010, with permission

class of compounds as well. The potent neuroprotective benefits for unmyelinated axon conduction, observed after a preinjury treatment with FK506, were absent when the immunophilin ligands were administered after the injury. In contrast, functioning of the myelinated axon improved with either preinjury or postinjury drug treatment. This pattern of results would be expected if unmyelinated callosal axons are, in fact, more vulnerable to the FPI than are the myelinated axons. At least for the two test drugs, FK506 and CsA, it would appear that the unmyelinated fibers receive a benefit if the drug is present at the time of injury, but these small axons may sustain sufficient damage that a treatment delayed by only 15 min may not prevent TBI-induced functional compromises. Our working interpretation of these results, taken together, is that structural disparities discussed in the introduction to this chapter (refer back to Fig. 15.1) place unmyelinated axons at a disproportionate risk to TBI. The high membrane content, small cytoplasmic buffering volume and axolemmal exposure, of unmyelinated axons, may present special challenges as drug treatments and interventions are developed and tested.

15.6 Fiber Type as a Factor in Posttraumatic Degradation of the Membrane Skeleton

To this point in the discussion, the presence or absence of myelin has been suggested as a fundamental factor in determining the axonal response to injury. Closely allied to this concept is the idea that myelinated axons may be most vulnerable to TBI at nodal regions that lack myelin. Nodes of Ranvier may be susceptible to injury for reasons beyond the simple lack of structural support and cushioning otherwise provided by myelin. Nodes are characterized by complex and spatially organized molecular domains that regulate axo–glial interactions (reviews: Scherer 1999; Bhat 2003; Susuki and Rasband 2008a). Damage at the paranodal loops, or the cell adhesion molecules that stabilize these contacts, would be predicted to elevate the risk of myelinated axons to the deleterious effects of secondary axonal injury, by exposing internodal axolemma to the aberrant extracellular environment which arises after TBI.

Molecular domains at nodes interact with the "membrane skeleton," a network of spectrin and related molecules located on the cytoplasmic surface of the axolemma. Multiple laboratories have identified a consistent feature of traumatic axonal injury to be the proteolysis of sub-axolemmal spectrin, mediated by the calpain family of calcium-dependent neutral proteases (Newcomb et al. 1997; Saatman et al. 2003; Hall et al. 2005; Park et al. 2007). Spectrin is attached to the plasma membrane through interactions with ankyrin. However, injury-induced changes in ankyrin have not, until recently, been systematically investigated. Although ankyrin proteins were once regarded as passive "linker" molecules, mounting evidence demonstrates they have diverse binding partners and complex roles which may involve them in the deleterious molecular breakdowns occurring after TBI. Ankyrins interact with the cytoplasmic domains of ion channels (Wood and Slater 1998; Malhotra et al. 2002),

transporters (Li et al. 1993; Michaely and Bennett 1995), Na+K+-ATPase (Davis and Bennett 1990; Devarajan et al. 1994), cell adhesion molecules (Dubreuil et al. 1996), and some classes of receptors (Bourguignon and Jin 1995; Hayashi and Su 2001). In the mammalian CNS, there is evidence that ankyrins stabilize the nodal and paranodal structure of myelinated axons. This stabilizing role is implemented not only through spectrin, but also through interactions with transmembrane neurofascins (reviewed in Susuki and Rasband 2008a). Ankyrins are directly involved with the clustering of voltage-gated sodium channels (NaVs) within axonal initial segments and at Nodes of Ranvier (Kordeli et al. 1995; Davis et al. 1996; Zhou et al. 1998; Rasband et al. 1999). With this increasing appreciation for the multifunctional nature of ankyrin proteins, came the need to examine the ankyrin response during the pathogenesis of TBI.

15.6.1 Ankyrin-G and αII-Spectrin Breakdown: A Comparison in Gray vs. White Matter

Our laboratory examined changes in ankyrin-G and αII-spectrin expression following FPI in adult rats (Reeves et al. 2010), assessing these proteins in CC and in cerebral cortex during the postinjury time interval of 3 h to 7 days. Our analyses were directed at whether ankyrin-G undergoes a proteolytic fragmentation comparable to that observed for spectrin. This study was also the first to explicitly compare the injury response of these membrane cytoskeletal proteins in white versus gray matter.

Our Western blot analyses of ankyrin-G focused on TBI-induced changes to three immunopositive bands (220, 212, 75 kDa), corresponding to proteolyzed fragments of the intact protein. These changes were strikingly restricted to the CC, with little or no change observed in the cortical samples. Callosal ankyrin-G alterations elicited by the FPI followed a consistent pattern of early (3 h to 1 day) surges in protein levels, and then resolving to control levels at 3–7 days. The 75 kDa band departed from this general profile, evolving from early postinjury increases to significantly depressed levels at 3–7 days (Fig. 15.18a). In cortical samples, the major pattern for all ankyrin bands was to remain near control levels (Fig. 15.18b), with a possible exception being a 61 % increase in the 220 kDa band at 1 day, although this was not statistically significant.

Western blot analyses of αII-spectrin showed antibody recognition of five major bands, migrating at 280, 180, 150, 145, and 120 kDa. Although alterations in spectrin protein after TBI were relatively larger in cortex than in CC, the time course of these changes was quite similar in the two regions (Fig. 15.19a, b). The most prominent feature was a marked upsurge in the calpain-derived 145 kDa αII-spectrin fragment, peaking at 3 days, but declining by 7 days to a level not significantly different from controls. A comparable time course was observed for the 150 kDa αII-spectrin fragment, which may represent a mix of fragments from calpain and caspase-3 activity (Wang 2000; Aikman et al. 2006). Notably, the 120 kDa caspase-3 derived breakdown product was essentially unchanged after TBI.

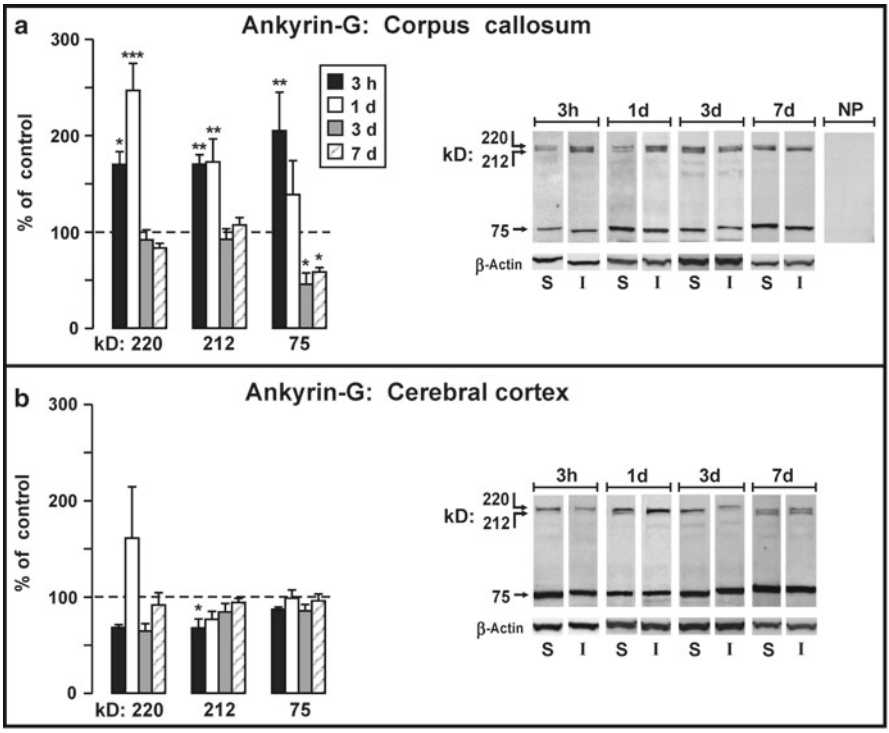

Fig. 15.18 Western blot analysis of ankyrin-G fragments following FPI. Data are plotted as percent change (mean +/− SEM) from sham-injured control rats at survival intervals 3 h, 1 day, 3 days, and 7 days. (**a**) In the CC, a significant surge was observed in 220 and 212 kDa ankyrin-G, which recovered to control levels on 3 and 7 days. The 75 kDa ankyrin-G product was significantly elevated at 3 h postinjury, but decreased to levels significantly below controls at 3 and 7 days. (**b**) The injury produced relatively minor changes in levels of ankyrin-G fragments in the parieto-temporal cortex, with the singular significant change being a 32 % decrease noted for the 212 kDa band measured at 3 h postinjury. From Reeves et al. 2010, with permission

An overall comparison, of ankyrin and spectrin modifications after TBI, suggests a surprising divergence in the response of these proteins to injury. Despite the well-established molecular binding of ankyrin and spectrin (Srinirasan et al. 1988; Kordeli and Bennett 1991; Kordeli et al. 1995; Susuki and Rasband 2008b), TBI produced dissimilar changes in these two proteins along several different dimensions: time course, magnitude of effect, and white matter specificity. First, changes in ankyrin-G showed a comparatively rapid time course, with significant increases confined to 3 h to 1 day, whereas alterations in αII-spectrin levels developed more slowly, and peaked at 3 days. Interestingly, among all immunopositive bands in the study, only the 75 kDa ankyrin-G fragment evolved from an early upsurge to a late (3–7 days) suppression significantly below controls. Secondly, the magnitude of changes in these proteins was quite disparate. The largest increase in αII-spectrin

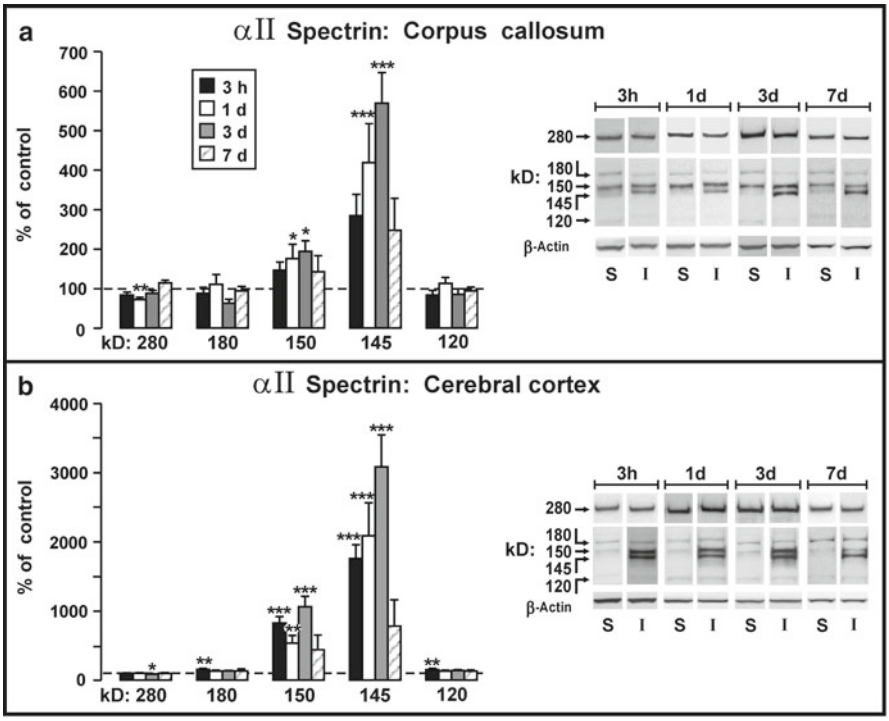

Fig. 15.19 Western blot analysis of αII-spectrin following FPI. Data are plotted as percent change from sham-injured control rats at survival intervals 3 h, 1 day, 3 days, and 7 days. (**a**) Analysis of αII-spectrin and fragments in the CC indicated an injury response primarily mediated by calpain proteolysis, with significant increases at 1 and 3 days in the 145/150 kDa products. No significant injury related changes were found for the 120 kDa fragment associated with caspase-3 activity. (**b**) Analysis of αII-spectrin and fragments in the parieto-temporal cortex revealed massive increases in the 145/150 kDa fragments, exceeding control levels by approximately 30-fold at 3 days postinjury. From Reeves et al. 2010, with permission

levels (+30-fold in 145 kDa) far exceeded the most sizeable change in ankyrin-G (+2.5-fold in 220 kDa). Thirdly, injury-induced changes in spectrin were clearly expressed in both cerebral cortex and CC, whereas the ankyrin response was a singularly white matter phenomenon.

The ankyrin-G protein is likely to be critical to axonal electrophysiology, through its role in spatially organizing ion channels and transporters essential for bioelectric function, and securing diverse proteins integral to the axolemma. For these reasons, and in view of the white matter specificity of post-TBI ankyrin changes, it was reasonable to consider if postinjury alterations to ankyrin proteins could be related to changes in CAP function previously observed to follow TBI (Reeves et al. 2005). Related to the issue of conduction deficits disproportionately affecting unmyelinated axons, there were reports which suggested the expression of distinct ankyrin isoforms within unmyelinated axons (Kordeli and Bennett 1991; Kordeli et al. 1995;

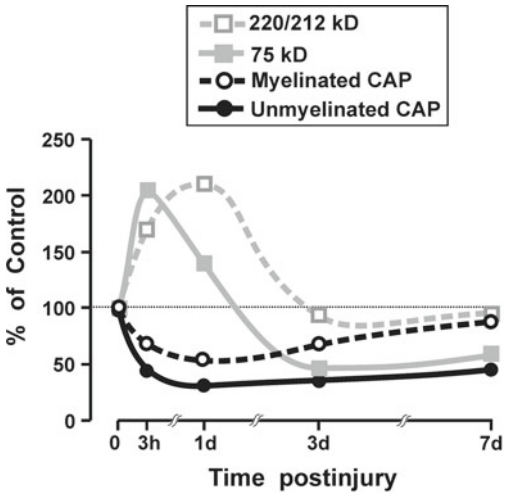

Fig. 15.20 Comparison of ankyrin-G Western blot results with prior measurements (Reeves et al. 2005) of CAP amplitudes recorded from the CC. All data are normalized as percent of sham-injured control levels. Data for the 220 and 212 kDa ankyrin-G fragments are pooled together. Several features of this graphical comparison suggest an association of the 220/212 kDa fragments with myelinated axons, and the 75 kDa product with unmyelinated axons. From Reeves et al. 2010, with permission

Peters et al. 1995; Rubtsov and Lopina 2000). To explore these issues, it was useful to replot the CAP amplitude data along with the measurements of ankyrin-G fragments, with all data normalized to uninjured control values (Fig. 15.20). For this comparison, the results for the 220 and 212 kDa ankyrin-G bands were averaged together, because they migrated in the gel as a doublet, and exhibited similar profiles of postinjury change. These plots suggested the hypothesis that there may be an association of the ankyrin fragments with postinjury CAP alterations. Injury effects reached a peak, for both protein levels and evoked CAPs, at the earlier (3 h to 1 day) time points. However, at 3 and 7 days the myelinated CAP component and the 220/212 kDa ankyrin level exhibit a return to control levels. A contrasting pattern was seen for the unmyelinated CAP signal and levels of the 75 kDa ankyrin, both of which remained significantly below control levels. It is conceivable that the upsurge and resolution of ankyrin 220/212 represents breakdown and clearance of higher isoforms of ankyrin, specifically the 270-kDa and 480-kDa isoforms of ankyrin-G which are highly localized to myelinated axons. In contrast, time-dependent changes in levels of the 75-kDa form may represent primarily a breakdown of the 190-kDa ankyrin-G, which has been associated with unmyelinated axons (reviewed in Rubtsov and Lopina 2000), although the possibility that some of the 75-kDa surge reflects residual fragments of the 270/480 kDa forms cannot be eliminated based on existing data. The processes leading to the rapid postinjury increase at 3 h in the 75 kDa fragment may be distinct from the reductions below control levels observed at 3 and 7 days. Specifically, the 3–7 days decreases indicate some constitutive

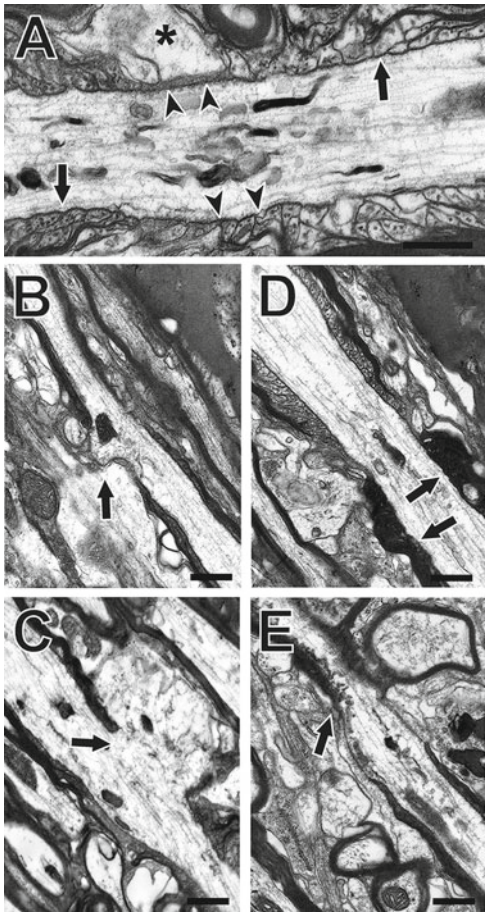

Fig. 15.21 Effect of FPI on Node of Ranvier ultrastructure in CC: (**a**), sham-injured control, (**b**–**e**), injured cases. Sham controls show typical nodal cytoarchitecture, with intact axolemmal membranes (*arrowheads* in (**a**)), normal profiles of adjacent paranodal loops (*arrows* in (**a**)) and axonal/glial interfaces (*asterisk* in (**a**)). Following injury, the axolemma is disrupted, with sites of extruded axonal cytoplasm visible (*arrows* in (**b**, **c**)), in some cases showing shifts of axial cytoskeleton into these regions. Further, paranodal loops of injured cases may appear abnormally electron dense (*arrows* in (**d**)), or show clear membrane disorganization (*arrows* in (**e**)). Bars = 0.5 μm. From Reeves et al. 2010, with permission

presence for 75 kDa ankyrin-G, and the loss of this protein may contribute to the persistent suppression of conduction in unmyelinated axons.

Concurrent with our evaluations of the membrane skeleton proteins, we also identified ultrastructural changes after FPI indicative of axonal pathology, characterized by compaction of axonal cytoskeleton, and damage to Nodes of Ranvier (Reeves et al. 2010). This approach was different from the ultrastructural stereology, conducted on axons in cross-section, as described above. Here, fibers viewed in longitudinal section exhibited nodal abnormalities appearing as cytoplasmic extravasations, or nodal blebs, as previously described in an optic nerve model of axonal injury (Maxwell et al. 1991). In control CC the axolemma was continuous across the node, exhibiting intact paranodal loops and normal nodal interface with glial processes (Fig. 15.21a). This contrasted with injured axonal profiles, which showed evidence of disrupted sub-membrane cytoarchitecture and axolemmal disorganization at the node, often presenting with expansion of axoplasm into the extracellular space (Fig. 15.21b, c). In some cases paranodal loops exhibited

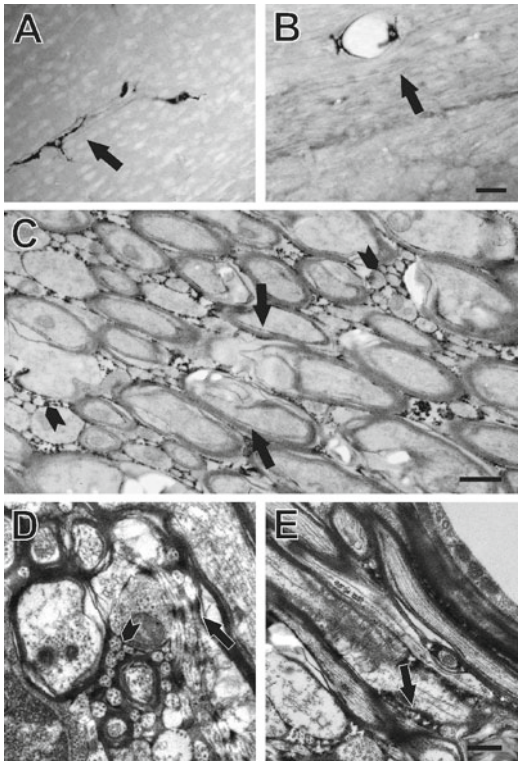

Fig. 15.22 Effects of FPI on white matter BBB disruption and nodal integrity. (**a**) Low magnification view of CC from control case infused with HRP 1 h before sham-injury. Intact BBB retards extravasation of HRP into neuropil, with tracer restricted to the callosal vasculature (*arrow*). (**b**) CC from animal administered HRP 1 h prior to FPI and sacrificed 24 h postinjury. Movement of HRP from vascular bed into space around axons is evident throughout the white matter (*arrow*). (**c**) Ultrastructure of noncounterstained injured case showing HRP diffusion into extracellular space around small unmyelinated fibers (*arrowheads*) and within the submyelin space between axolemma and inner myelin sheath (*arrows*). (**d**, **e**) Higher magnification of counterstained ultrastructure from an injured case. In D, HRP localization is seen around axon bundles (*arrowhead*) and along the surface of glial membranes (*arrows*) and infiltrating paranodal/submyelin space at *arrow* in (**e**) Bar = 30 μm in (**a**, **b**); 10 μm in (**c**); 0.5 μm in (**d**, **e**). From Reeves et al. 2010, with permission

darkened, floccular cytoplasm (Fig. 15.21d), while other injured axons displayed paranodal membrane degeneration (Fig. 15.21e).

Throughout our investigations, of fiber type as a factor in injury outcome, it has been useful to consider if axon populations differ with respect to the degree of axolemmal exposure to aberrant ionic and proteolytic conditions prevailing in the extracellular compartment after injury. This includes extravasating factors that gain parenchymal access in blood–brain barrier (BBB) failures that often accompany TBI. We examined BBB disruption in CC at 1 day postinjury, showing that horseradish peroxidase (HRP), normally retained within brain vasculature, had passed through the vessel walls and entered into the extracellular space around myelinated and unmyelinated fibers (Fig. 15.22). Movement of HRP into the submyelin space, adjacent to

damaged axolemma of myelinated axons, was also evident, and comparable to a pathological pattern previously reported in brainstem white matter tracts after impact acceleration injury (Pettus et al. 1994). At low magnification, the HRP tracer was observed confined within CC vasculature in control tissue, but extruded into the parenchyma of injured animals (Fig. 15.22a, b). When unstained thin sections were examined ultrastructurally, HRP was extensively distributed within the spaces surrounding myelinated axons and outlining bundles of small unmyelinated fibers (Fig. 15.22c). This view also revealed a thin band of tracer between myelin sheath and the axolemma of some fibers (the "submyelin space"). In counterstained thin sections, HRP was observed reaching the extracellular interface between myelinated and unmyelinated axons, and spaces surrounding glial processes (Fig. 15.22d). At injured nodes, HRP appears to fill the space around paranodal loops and extends further along the juxtaparanodal axon/glial interface (Fig. 15.22e). We concluded from these observations, that damaged nodes exhibiting compromised cytoskeletal integrity and membrane adhesion may permit exposure to molecules normally excluded from the internodal axolemma.

15.7 Extracellular Matrix Molecules are Mediators of Axonal Injury and Recovery

Given that our HRP studies in the injured CC revealed the extracellular matrix as a conduit for molecules mediating axonal pathology, we have begun to explore the potential for secreted matrix metalloproteinases (MMPs) to regulate the evolution of this pathology through their matrix/axolemma interaction. These Ca^{++}/Zn^{++} activated enzymes control the organization of the protein matrix around axons, and they are activated by molecules like tissue plasminogen activator (tPA) and circulating cytokines, which are released into that matrix with BBB disruption (Gurney et al. 2006 ; Seo et al. 2012). Prior studies of CNS insult point to MMPs as having the potential to generate axon pathology, not only in TBI (Truettner et al. 2005; Vilalta et al. 2008; Li et al. 2009), but after stroke and ischemia (Suzuki et al. 2007; Walker and Rosenberg 2009; Park et al. 2009), as well as with multiple sclerosis (MS) white matter degeneration (Rosenberg et al. 2001; Kanesaka et al. 2006; Yong et al. 2007) and spinal cord injury (Noble et al. 2002; Hsu et al. 2006). Further, studies of tissue disruption and repair following CNS trauma support a critical role for MMP substrates such as agrin (Solé et al. 2004; Falo et al. 2008), tenascin (Zhang et al. 1997; Hausmann and Betz 2001), phosphacan (Jones et al. 2003; Harris et al. 2011), versican (Asher et al. 2002; Harris et al. 2009) and neurofascin (Mathey et al. 2007; Reeves et al. 2010; Pomicter et al. 2010), each of which is well positioned to influence axolemma stability and axonal integrity. These matrix proteases are not only associated with axonal pathology, but also contribute to the extent of postinjury recovery (Yong 2005; Ahmed et al. 2005; Hsu et al. 2006). Moreover, their targeted inhibition can attenuate both structural and functional damage after CNS trauma, facilitating improved recovery (Falo et al. 2006; Homsi et al. 2009; Warren et al. 2012). In the context of brain injury, MMPs also have the potential to alter BBB stability (Lin et al. 2012; Higashida et al. 2011), as well as influence immune

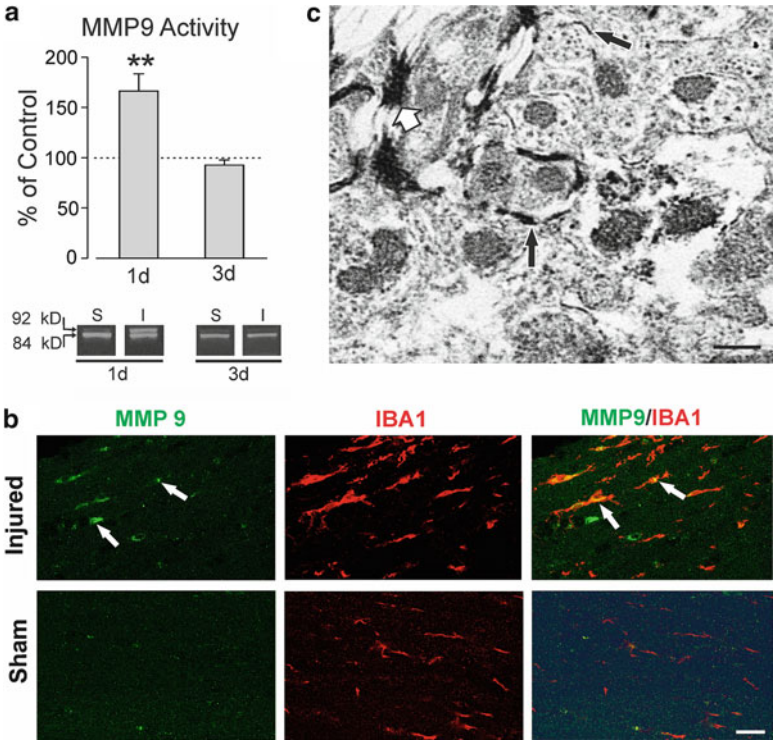

Fig. 15.23 MMP expression and distribution in CC following FPI. (**a**) Gelatin zymography of CC extracts after FPI showed significant acute elevation in 92 kDa pro MMP9 at 1 day postinjury and a return to sham control levels by 3 days ($n = 7–15$/group). (**b**) Confocal co-label experiments illustrate increased CC MMP9 at 1 day postinjury relative to sham controls, consistent with elevated pro MMP9 activity detected by zymography. Principal MMP9 tissue signal was found within reactive microglia (*arrows in overlay*). (**c**) Ultrastructural immunocytochemistry for CC MMP3 at 3 days after FPI revealed enzyme distribution among damaged axons. Noncounterstained sections showed MMP3 reaction product around unmyelinated axons (*black arrows*) and within disrupted myelin sheaths (*white arrowhead*). This MMP distribution is consistent with HRP identified sites where extravasated molecules were redistributed among CC axons following FPI. $*p<0.01$; Bar = 10 μm in (**b**), 0.5 μm in (**c**)

signaling between neurons and neuroglia (Agrawal et al. 2006; Csuka et al. 2000; Morganti-Kossmann et al. 2007).

Based upon our prior studies with injured gray matter (Falo et al. 2006; Phillips and Reeves 2001), we first tested gelatinase B (MMP9) and stromelysin-1 (MMP3) as candidates for callosal matrix activation after TBI. Zymographic analysis (Fig. 15.23a) showed a significant 66.3 % increase of 92 kDa pro MMP9 activity over sham controls at 1 day, but no change at 3 days postinjury. Confocal labeling experiments support elevated callosal MMP9 at 1 day after TBI, with colocalization of the enzyme in IAB1+ microglia (Fig. 15.23b) and GFAP + astrocytes (data not shown). Acute rise in MMP9 is consistent with published elevation of gelatinase

activity in gray matter and plasma after TBI (Muir et al. 2002; Grossetete et al. 2009), and is thought to underlie the onset of BBB permeability in models of stroke, TBI and spinal cord injury (Seo et al. 2012; Candelario-Jalil et al. 2011; Shigemori et al. 2006). Notably, white matter degeneration produced by MS and experimental autoimmune encephalomyelitis (EAE) display the common phenotype of exacerbated MMP9 proteolysis (Leppert et al. 1998; Gijbels et al. 1993).

A similar up regulation of MMP3 was reported in degenerative white matter tracts of patients with vascular dementia (Rosenberg et al. 2001) and MS (Cuzner et al. 1996; Anthony et al. 1997), and in a mouse model of spontaneous demyelination (D'Souza et al. 2002). Injury-induced increase of MMP3 is described following transection of optic axons (Agapova et al. 2003), and the enzyme is elevated in both rodent cortical contusion models (Li et al. 2009), as well as in the serum of MS patients with relapsing-remitting demyelination (Kanesaka et al. 2006). In preliminary Western blot studies, CC MMP3 protein expression was higher after injury, but this change did not reach significance when compared to sham controls (data not shown). Although the time course of MMP3 activity following TAI is not yet documented, we have applied ultrastructural immunocytochemistry to track its distribution in the CC, and our results demonstrate that MMP3 is localized among disrupted axonal profiles 3 days after callosal injury (Fig. 15.23c). Together, these data support an active role for secreted MMPs in the evolution of TAI and point to the potential benefit of MMP inhibition during the early phases of axonal injury.

While MMP inhibition has been demonstrated to affect recovery after vascular insult (Romanic et al. 1998; Asahi et al. 2000; Zhao et al. 2006), spinal cord or sciatic nerve injury (Wells et al. 2003; Busch et al. 2009; Liu et al. 2010), neurodegenerative disease (Yong et al. 2007), and axotomy induced deafferentation (Reeves et al., 2003; Falo et al. 2006; Warren et al. 2012), the specific effects of blocking MMP activity during the evolution of white matter pathobiology are not well understood. Recently we have used literature supported strategies to inhibit MMP9 and MMP3 following FPI in order to test the effect of this inhibition on callosal MMP activity and CAP deficits. One of the most efficient modulators of MMP9 activity for both stroke and MS has been the tricyclic antibiotic minocycline (Murata et al. 2008; Yenari et al. 2006; Giuliani et al. 2005). Although the drug is pleiotropic, it clearly targets MMP9 functional activity (Romero-Perez et al. 2008; Murata et al. 2008; Homsi et al. 2009). In the context of TBI, reports exploring minocycline efficacy have been mixed. Postinjury minocycline dosing after both weight drop (Bye et al. 2007) and impact acceleration (Homsi et al. 2009) TBI does appear to reduce microglial inflammatory response and cell death, as well as improve neurological outcome. By contrast, in the controlled cortical impact model, minocycline failed to improve cognitive deficits (Kelso et al. 2011), suggesting that minocycline protective effect may be complex and model dependent. Interestingly, when minocycline was delivered in combination with N-actyelcysteine in the latter model, a selective neuroprotection of white matter was observed (Baki et al. 2010). This beneficial effect of minocycline was in direct contrast to that reported by Homsi et al. (2010) after impact acceleration, where the drug did not alter APP deposition in large caliber myelinated axons exhibiting TAI. We hypothesized that these discrepancies in

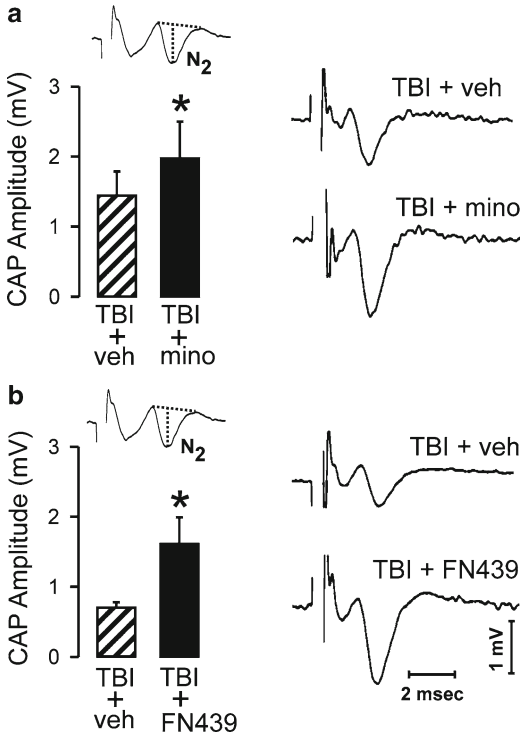

Fig. 15.24 Effect of MMP inhibitors (minocycline and FN439) on mean CAP amplitudes measured following FPI. Injury-induced suppression of CC unmyelinated CAP amplitude (mean post-TBI CAP amplitude shown as TBI + veh bars in (**a**, **b**)) was significantly reversed by either minocycline treatment (TBI + mino in (**a**)) or FN439 treatment (TBI + FN439 in (**b**)). Representative CAPs are shown at *right*. Neither MMP inhibitor significantly altered the amplitude of the mean myelinated CAP signal (N1) following TBI (not shown). *$p<0.05$, $n = 4–6$/group

minocycline efficacy may be due to the fact that the drug preferentially protects smaller caliber unmyelinated fibers through inhibition of matrix MMP9 pathways.

To test this hypothesis we first applied minocycline (45 mg/kg, i.p.; 30 min, 6 h) after moderate midline FPI and probed for effect on callosal gelatinase activity at 1 and 3 days postinjury. While minocycline failed to alter 92 kDa pro MMP activity, the drug significantly reduced proteolysis in the tightly regulated 84 kDa active form of MMP9 by 23.6 ± 8.7 % at 1 day. We observed no effect of minocycline treatment on MMP9 activity at 3 days survival. Next we examined CAP response in myelinated and unmyelinated fiber populations of the CC following minocycline treatment, increasing the dosing to 90 mg/kg i.p., delivered again at 30 min, 6 h postinjury. As for FK506 and CsA experiments, CAP amplitude was used to determine injury and drug effect. Figure 15.24a shows aggregate histograms of N2 callosal CAP response at maximal stimulus intensities, where we found that minocycline significantly reduced injury-induced CAP deficits in the unmyelinated fiber population, an effect present at 1 day, but not at 3 days survival. Minocycline had no effect on callosal myelinated fiber CAP deficits (data not shown). These CAP data are consistent with our zymographic results showing minocycline reduction of callosal MMP9 activity at 1 day but not 3 days after TBI.

In a second set of experiments we tested the effect of targeted MMP3 inhibition on callosal fiber function using MMP inhibitor I (FN439). While available MMP

inhibitors are not entirely selective, we have shown that FN439 can attenuate MMP3 functional activity by 40 % in gray matter deafferented by axonal lesion (Kim et al. 2005). We also know that FN439 attenuates synaptic degeneration resulting from this axonal lesion (Falo et al. 2006). Other published applications of FN439 to brain injury have been limited to models of physiological synaptic plasticity (Reeves et al., 2003; Meighan et al. 2007; Wójtowicz and Mozrzymas 2010) or behavioral assessments of spatial memory (Wright et al. 2007). To our knowledge, no studies have utilized FN439 to manipulate MMP3 within the injured CC, nor has the effect of FN439 on CAP deficits been tested. In pilot plate assays we found that lytic activity attributable to MMP3 within injured callosal extracts was blocked with exposure to FN439 (unpublished observations), supporting its application to inhibit MMP3 in white matter tracts. When rats were subjected to midline moderate FPI and treated 30 min postinjury with FN439 (10 mg/kg, i.v.), deficits in N2 CAP amplitude of unmyelinated axons were significantly reduced at 3 days survival (Fig. 15.24b). As with minocycline, myelinated CAP signal was not altered by FN439 exposure (data not shown). Given that MMP3 was pervasive among degraded unmyelinated axons at 3 days postinjury in our ultrastructural studies, FN439 would be predicted to significantly reduce 3 days N2 CAP deficits if MMP3 is involved in the axonal pathophysiology.

From these initial studies of MMP response following moderate FPI we conclude that both MMP9 and MMP3 contribute to the evolution of axonal pathology with DAI. The acute postinjury application of MMP inhibiting drugs can provide functional neuroprotection for injured unmyelinated axons, a response partially mediated through these two proteases. Finally, the fact that the beneficial effects of MMP inhibition target the fiber population with more exposed axonal membrane adds further support to the hypothesis that the interface between axons and extracellular matrix is a critical site for the maintenance of fiber integrity after TBI.

15.8 TBI Effects in a Predominantly Myelinated Fiber Tract: The Internal Capsule

On the basis of ultrastructural, electrophysiological, and molecular evidence, obtained from observations in CC, we conclude that fiber type is a significant determinant of outcome in axonal injury. However, it is essential to test the generality of this principle by examining how fiber type affects the properties of TAI in forebrain white matter other than the CC. One useful strategy will be to assess TAI in anatomical regions which are enriched in myelinated axons, with minimal unmyelinated fiber contribution. These types of comparative observations should help clarify the degree to which injury severity is related to the proportion of unmyelinated axons present. Although myelinated axons are susceptible to TAI, at all levels of the neuraxis, injury to white matter regions which are highly enriched in myelinated fibers should have a relatively small burden of dysfunctional, or structurally altered, unmyelinated axons. To address these issues our laboratory has initiated studies to

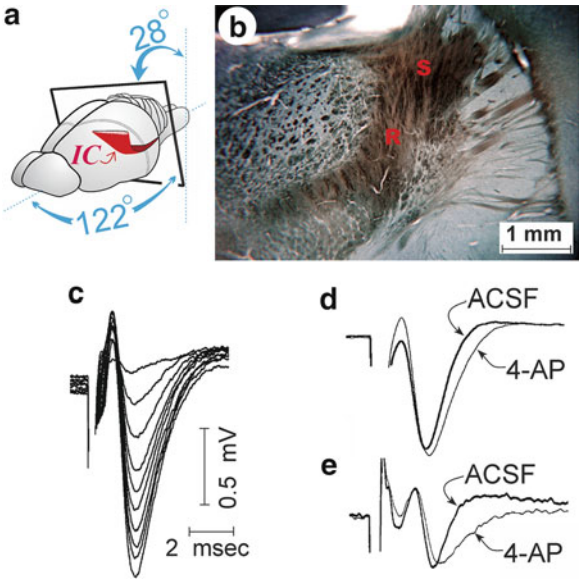

Fig. 15.25 CAP recording in internal capsule (IC). (**a**) Blocking angle for IC slice preparation. (**b**) Sudan Black-stained section showing location of stimulating "S" and recording "R" electrodes. (**c**) Graded stimulation generated family of monophasic CAPs. (**d**, **e**) Blockade of K^+ channels (4-AP), produced large increases in duration of unmyelinated CAPs in corpus callosum (**e**), but comparatively small increases in IC CAPs (**d**), consistent with preponderance of myelinated fibers in the IC

assess TAI in the internal capsule (IC), which is composed principally of large caliber myelinated axons. While posttraumatic damage to the brainstem portion of these fibers (Pettus et al. 1994; Povlishock 1992; Povlishock et al. 1997; Okonkwo et al. 1999; Buki et al. 1999, 2003; Singleton et al. 2001; Stone et al. 2001, 2002; Marmarou and Povlishock 2006), as well as thalamic branches (Singleton et al. 2002) have been well documented, studies examining structural and functional changes in the fibers further upstream have not been conducted.

In head injured patients, DAI lesions in the IC have been implicated in motor weakness following TBI (Choi et al. 2011). The diffusivity abnormalities, detected using DTI in CC of TBI patients, are also observed for the IC. Both regions exhibit reduced axial diffusivity, and increased radial diffusivity, following severe head injury (Sidaros et al. 2008; Betz et al. 2012). Injury also significantly reduced fractional anisotropy values in the IC and splenium (Arfanakis et al. 2002).

We have begun our investigation of functional changes in IC axons following TBI. An early step in this process was the development of IC brain slices for CAP recording. Due to the trajectory of the capsular axons, it was necessary to block the brains using a compound angle which maximally preserved the numbers of continuous longitudinal fibers within a slice (Fig. 15.25a). Using recording conditions identical to those of our callosal recording, we observed that stimulation of IC axons produced CAPs with a single negative-going phase (Fig. 15.25c). This was consistent with a largely homogeneous myelinated fiber population, and contrasted with the biphasic CAPs generated by the mixed myelinated and unmyelinated axons in CC. Further evidence confirming the predominant myelinated composition of the IC

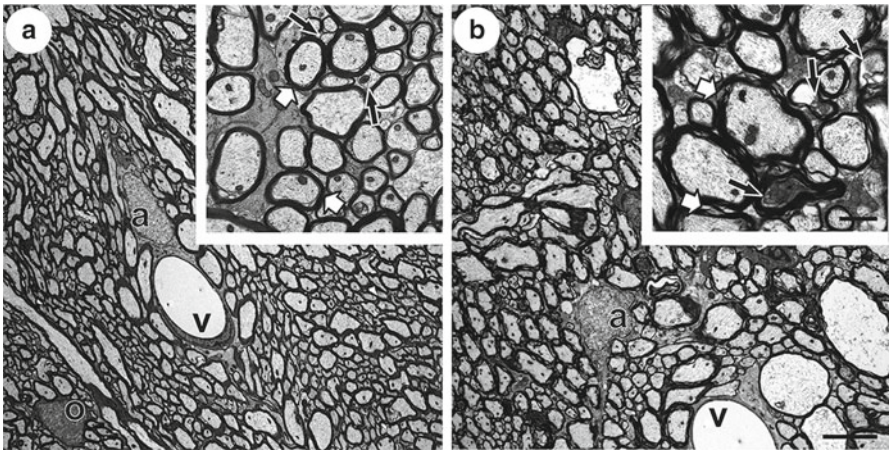

Fig. 15.26 Internal capsule axonal pathology at 3 days following FPI. (**a**) Ultrastructure of sham control IC showed intact axons, predominantly medium to large myelinated fibers. At higher magnification (inset in (**a**)) these fibers have intact myelin sheath and axoplasmic structure (*arrowheads*), with associated glial processes and interspersed unmyelinated axons (*arrows*). (**b**) At 3 days after FPI axonal pathology is observed in the myelinated population, with collapse of the axonal cytoplasm and myelin disruption. Under higher magnification (inset in (**b**)), injured axons showed a striking myelin sheath disruption, particularly in large caliber fibers (*arrowheads*). Axoplasm of injured axons was dark, collapsed and degraded (*arrows*). *a* astrocyte, *o* oligodendrocyte, *v* vessel; Bar = 5 μm in ((**a**, **b**) low magnification), 1 μm in each inset

was obtained in experiments where the slices were recorded after bath application of the K^+ channel blocker 4-AP. K^+ channels exposed on unmyelinated axolemma are readily affected by the 4-AP, which acts to prolong CAPs in unmyelinated axons. In the IC slices, 4-AP produced relatively small changes to CAP duration (Fig. 15.25d), especially compared to the broadening of the unmyelinated CAP observed in CC (Fig. 15.25e). Further, our initial stereological estimates of the relative proportions of myelinated and unmyelinated fibers in this region also indicate a chiefly myelinated tract. Specifically, using unbiased counting frames and sampling rules similar to those described above (Reeves et al. 2012), estimates in a preliminary set of rats ($n = 4$) indicated that 89.0 ± 5.2 % of the IC axons were myelinated. Example electron micrographs of the IC illustrate the fiber composition as principally medium to large diameter myelinated axons (Fig. 15.26a). An example of IC ultrastructure at 3 days following FPI suggests pathological cytoplasmic and myelin changes (Fig. 15.26b). In this case, FPI produced disruptions of the myelin sheath and dark collapsed cytoplasm (inset in Fig. 15.26b). Concurrent with our ongoing ultrastructural evaluation of TBI effects in the IC, we are in parallel assessing CAPs in this tract following midline FPI. In a pilot set of five rats (two sham injured, three TBI recorded at 3 days postinjury), we observed the average maximum CAP amplitude in TBI rats (0.56 ± 0.28 mV) to be suppressed relative to the sham level

(1.46 ± 0.08 mV; $p < 0.05$). We are confident that additional data acquisition using this slice model will lead to a greater understanding of how fiber composition influences functional changes after TBI.

15.9 Looking Forward: How Fiber-Type-Specific Vulnerability May Translate to Clinical Practice

From the clinical perspective, it is useful to consider if behavioral deficits, observed in head injured patients, may reflect damage sustained by specific populations of axons. While sensory and/or motor impairments may exert a devastating toll on some victims of TBI, it has long been recognized (e.g., Levin 1996) that cognitive and memory deficits are the most common, and enduring, problems facing head injury patients. Therefore, it is reasonable to examine evidence that axon populations subserving neocortical association areas may not be identical to those in pathways which are dedicated specifically to sensory or motor systems. In this context, morphometric studies of the CC in primates and humans have indicated that the composition of axon types varies among different callosal subregions. Specifically, the distribution of axon subtype, along the anteroposterior axis of the CC, is in register with projections from functionally and cytoarchitectonically distinct neocortical areas in rhesus monkey (Lamantia and Rakic 1990) and human (Aboitiz et al. 1992, 2003), and, notably, the callosal regions with the largest proportion of unmyelinated axons interconnect association cortex. It is conceivable that a postinjury loss of unmyelinated axons disproportionately impacts fibers subserving associative memory functions, with a relative sparing of sensorimotor-dedicated axons. In this scenario, damage to unmyelinated fibers may result in a transient functional deficit, or an actual numerical loss if they are not recoverable. In our studies, the primary morphometric parameter, axon caliber, transiently decreased only in unmyelinated axons after experimental TBI. A significant caliber reduction would be predicted to slow the velocity of axonal conduction, and correspondingly degrade information processing. A reduced unmyelinated axon caliber, followed by a recovery to normal dimensions, may significantly contribute to the common pattern of initial posttraumatic cognitive impairment, followed by some degree of improvement with the passage of time. We are confident that an increased understanding of the unmyelinated axon vulnerability to TBI, the evolution of their pathological features, and the unique response of these fibers to neuroprotective compounds, will facilitate the development of new therapeutic strategies.

Acknowledgements The authors wish to thank Terry Smith, Judy Williamson, Lesley Harris, Raiford Black, and Nancy Lee for their excellent technical assistance in this work. Supported by the National Institutes of Health (grants NS057758, NS056247, NS047463) and Virginia Commonwealth Neurotrauma Initiative 07–302 F. Microscopy was performed at VCU, Department of Anatomy and Neurobiology Microscopy Facility which is supported, in part, with funding from NIH-NINDS Center Core Grant NS047463.

References

Aboitiz F, Scheibel AB, Fisher RS et al (1992) Fiber composition of the human corpus callosum. Brain Res 598:143–153

Aboitiz F, Lopez J, Montiel J (2003) Long distance communication in the human brain: timing constraints for inter-hemispheric synchrony and the origin of brain lateralization. Biol Res 36:89–99

Adams JH, Doyle D, Ford I et al (1989) Diffuse axonal injury in head injury: definition, diagnosis and grading. Histopathology 15:49–59

Agapova OA, Kaufman PL, Lucarelli MJ et al (2003) Differential expression of matrix metalloproteinases in monkey eyes with experimental glaucoma or optic nerve transection. Brain Res 967:132–143

Agrawal S, Anderson P, Durbeej M et al (2006) Dystroglycan is selectively cleaved at the parenchymal basement membrane at sites of leukocyte extravasation in experimental autoimmune encephalomyelitis. J Exp Med 203:1007–1019

Ahmed Z, Dent RG, Leadbeater WE et al (2005) Matrix metalloproteases: degradation of the inhibitory environment of the transected optic nerve and the scar by regenerating axons. Mol Cell Neurosci 28:64–78

Ai J, Liu E, Wang J et al (2007) Calpain inhibitor MDL-28170 reduces the functional and structural deterioration of corpus callosum following fluid percussion injury. J Neurotrauma 24:960–978

Aikman J, O'Steen B, Silver X et al (2006) Alpha-II-spectrin after controlled cortial impact in the immature rat brain. Dev Neurosci 28:457–465

Anthony DC, Ferguson B, Matyzak MK et al (1997) Differential matrix metalloproteinase expression in cases of multiple sclerosis and stroke. Neuropathol Appl Neurobiol 23:406–415

Arfanakis K, Haughton VM, Carew JD et al (2002) Diffusion tensor MR imaging in diffuse axonal injury. Am J Neuroradiol 23:794–802

Asahi M, Asahi K, Jung JC et al (2000) Role for matrix metalloproteinase 9 after focal cerebral ischemia: effects of gene knockout and enzyme inhibition with BB-94. J Cereb Blood Flow Metab 20:1681–1689

Asher RA, Morgenstern DA, Shearer MC et al (2002) Versican is upregulated in CNS injury and is a product of oligodendrocyte lineage cells. J Neurosci 22:2225–2236

Baker AJ, Phan N, Moulton RJ et al (2002) Attenuation of the electrophysiological function of the corpus callosum after fluid percussion injury in the rat. J Neurotrauma 19:587–599

Baki SGA, Schwab B, Haber M et al (2010) Minocycline synergizes with N-acetylcysteine and improves cognition and memory following traumatic brain injury in rats. PLoS One 5:12490

Betz J, Zhou J, Roy A et al (2012) Prognostic value of diffusion tensor imaging parameters in severe traumatic brain injury. J Neurotrauma 29:1292–1305

Bhadelia RA, Price LL, Tedesco KL et al (2009) Diffusion tensor imaging, white matter lesions, the corpus callosum, and gait in the elderly. Stroke 40:3816–3820

Bhat MA (2003) Molecular organization of axo-glial junctions. Curr Opin Neurobiol 13:552–559

Bourguignon LY, Jin H (1995) Identification of the ankyrin-binding domain of the mouse T-lymphoma cell inositol 1,4,5-trisphosphate (IP3) receptor and its role in the regulation of IP3-mediated internal Ca2+ release. J Biol Chem 270:7257–7260

Buki A, Okonkwo DO, Povlishock JT (1999) Postinjury cyclosporin A administration limits axonal damage and disconnection in traumatic brain injury. J Neurotrauma 58:365–375

Buki A, Farkas O, Doczi T et al (2003) Preinjury administration of the calpain inhibitor MDL-28170 attenuates traumatically induced axonal injury. J Neurotrauma 20:261–268

Burke D, Mogyoros I, Vagg R et al (1998) Quantitative description of the voltage dependence of axonal excitability in human cutaneous afferents. Brain 121:1975–1983

Busch SA, Horn KP, Silver DJ et al (2009) Overcoming macrophage-mediated axonal dieback following CNS injury. J Neurosci 29:9967–9976

Butcher SP, Henshall DC, Teramura Y et al (1997) Neuroprotective actions of FK506 in experimental stroke: in vivo evidence against an antiexcitotoxic mechanism. J Neurosci 17:6939–6946

Bye N, Habgood MD, Callaway JK et al (2007) Transient neuroprotection by minocycline following traumatic brain injury is associated with attenuated microglial activation but no changes in cell apoptosis or neutrophil infiltration. Exp Neurol 204:220–233

Candelario-Jalil E, Thompson J, Taheri S et al (2011) Matrix metalloproteinases are associated with increased blood–brain barrier opening in vascular cognitive impairment. Stroke 42: 1345–1350

Cederberg D, Siesjo P (2010) What has inflammation to do with traumatic brain injury? Childs Nerv Syst 26:221–226

Choi GS, Kim OL, Kim SH et al (2011) Classification of cause of motor weakness in traumatic brain injury using diffusion tensor imaging. Arch Neurol 69:363–367

Colley BS, Phillips LL, Reeves TM (2010) The effects of cyclosporin-A on axonal conduction deficits following traumatic brain injury in adult rats. Exp Neurol 224:241–251

Csuka E, Hans VH, Ammann E et al (2000) Cell activation and inflammatory response following traumatic axonal injury in the rat. Neuroreport 11:2587–2590

Cuzner ML, Gveric D, Strand C et al (1996) The expression of tissue-type plasminogen activator, matrix metalloproteases and endogenous inhibitors in the central nervous system in multiple sclerosis: comparison of stages in lesion evolution. J Neuropathol Exp Neurol 55:1194–1204

Davis JQ, Bennett V (1990) The anion exchanger and Na+K(+)-ATPase interact with distinct sites on ankyrin in in vitro assays. J Biol Chem 265:17252–17256

Davis JQ, Lambert S, Bennett V (1996) Molecular composition of the node of Ranvier: identification of ankyrin-binding cell adhesion molecules neurofascin (mucin+/third FNIII domain-) and NrCAM at nodal axon segments. J Cell Biol 135:1355–1367

Devarajan P, Scaramuzzino DA, Morrow JS (1994) Ankyrin binds to two distinct cytoplasmic domains of Na, K-ATPase alpha subunit. Proc Natl Acad Sci U S A 91:2965–2969

DiLeonardi AM, Huh HW, Raghupathi R (2009) Impaired axonal transport and neurofilament compaction occur in separate populations of injured axons following diffuse brain injury in the immature rat. Brain Res 1263:174–182

Dixon CE, Lyeth BG, Povlishock JT et al (1987) A fluid percussion model of experimental brain injury in the rat. J Neurosurg 67:110–119

D'Souza CA, Mak B, Moscarello MA (2002) The up-regulation of stromelysin-1 (MMP-3) in a spontaneously demyelinating transgenic mouse precedes onset of disease. J Biol Chem 277: 13589–13596

Dubreuil RR, MacVicar G, Dissanayake S et al (1996) Neuroglian-mediated cell adhesion induces assembly of the membrane skeleton at cell contact sites. J Cell Biol 133:647–655

Evans PH (1993) Free radicals in brain metabolism and pathology. Br Med Bull 49:577–587

Eyer J, Leterrier JF (1988) Influence of the phosphorylation state of neurofilament proteins on the interactions between purified filaments in vitro. Biochem J 252:655–660

Falo MC, Fillmore HL, Reeves TM et al (2006) MMP3 expression profile differentiates adaptive and maladaptive synaptic plasticity induced by brain injury. J Neurosci Res 84:768–781

Falo MC, Reeves TM, Phillips LL (2008) Agrin expression during synaptogenesis induced by traumatic brain injury. J Neurotrauma 25:769–783

Geffen GM, Jones DL, Geffen LB (1994) Interhemispheric control of manual motor activity. Behav Brain Res 64:131–140

Gentry LR, Thompson B, Godersky JC (1988) Trauma to the corpus callosum: MR features. AJNR Am J Neuroradiol 9:1129–1138

Gijbels K, Proost P, Masure S et al (1993) Gelatinase B is present in the cerebrospinal fluid during experimental autoimmune encephalomyelitis and cleaves myelin basic protein. J Neurosci Res 36:432–440

Giuliani F, Metz LM, Wilson T et al (2005) Additive effect of the combination of glatiramer acetate and minocycline in a model of MS. J Neuroimmunol 158:213–221

Gorrie C, Duflou J, Brown J et al (2001) Extent and distribution of vascular brain injury in pediatric road fatalities. J Neurotrauma 18:849–860

Goto S, Yamamoto H, Fukunaga K et al (1985) Dephosphorylation of microtubule-associated protein 2, tau factor, and tubulin by calcineurin. J Neurochem 45:276–283
Graham DI, McIntosh TK, Maxwell WL et al (2000) Recent advances in neurotrauma. J Neuropathol Exp Neurol 59:641–651
Gravel C, Sasseville R, Hawkes R (1990) Maturation of the corpus callosum of the rat: II. Influence of thyroid hormones on the number and maturation of axons. J Comp Neurol 291:147–161
Grossetete M, Phelps J, Arko L et al (2009) Elevation of matrix metalloproteinases 3 and 9 in cerebrospinal fluid and blood in patients with severe traumatic brain injury. Neurosurgery 65:702–708
Gurney KJ, Estrada EY, Rosenberg GA (2006) Blood–brain barrier disruption by stromelysin-1 facilitates neutrophil infiltration in neuroinflammation. Neurobiol Dis 23:87–96
Hall ED, Sullivan PG, Gibson TR et al (2005) Spatial and temporal characteristics of neurodegeneration after controlled cortical impact in mice: more than a focal brain injury. J Neurotrauma 22:252–265
Harris NG, Carmichael ST, Hovda DA et al (2009) Traumatic brain injury result in disparate regions of chondroitin sulfate proteoglycan expression that are temporally limited. J Neurosci Res 87:2937–2950
Harris JL, Reeves TM, Phillips LL (2011) Phosphacan and receptor protein tyrosine Phosphatase β expression mediates deafferentation-induced synaptogenesis. Hippocampus 21:81–92
Hausmann R, Betz P (2001) Course of glial immunoreactivity for vimentin, tenascin and alpha1-antichymotrypsin after traumatic injury to human brain. Int J Legal Med 114:338–342
Hayashi T, Su TP (2001) Regulating ankyrin dynamics: roles of sigma-1 receptors. Proc Natl Acad Sci U S A 98:491–496
Higashida T, Kreipke CW, Rafols JA et al (2011) The role ofh y poxia-inducible factor-1α, aquaporin-4, and matrix metalloproteinase-9 in blood-brain barrier disruption and brain edema after traumatic brain injury. J Neurosurg 114:92–101
Hodgkin AL, Huxley AF (1952) A quantitative description of membrane current and its application to conduction and excitation in nerve. J Physiol 117:500–544
Homsi S, Federico F, Croci N et al (2009) Minocycline effects on cerebral edema: relations with inflammatory and oxidative stress markers following traumatic brain injury in mice. Brain Res 1291:122–132
Homsi S, Piaggio T, Croci N et al (2010) Blockade of acute microglial activation by minocycline promotes neuroprotection and reduces locomotor hyperactivity after closed head injury in mice: a twelve-week follow-up study. J Neurotrauma 27:911–921
Hsu JY, McKeon R, Goussev S et al (2006) Matrix metalloproteinase-2 facilitates wound healing events that promote functional recovery after spinal cord injury. J Neurosci 26:9841–9850
Iwata A, Stys PK, Wolf JA et al (2004) Traumatic axonal injury induces proteolytic cleavage of the voltage-gated sodium channels modulated by tetrodotoxin and protease inhibitors. J Neurosci 24:4605–4613
Jafari SS, Maxwell WL, Neilson M et al (1997) Axonal cytoskeletal changes after non-disruptive axonal injury. J Neurocytol 26:207–221
Jafari SS, Maxwell WL, Neilson M et al (1998) Axonal cytoskeletal changes after non-disruptive axonal injury: II. Intermediate sized axons. J Neurotrauma 15:955–966
Jones LL, Margolis RU, Tuszynski MH (2003) The chondroitin sulfate proteoglycans neurocan, brevican, phosphacan, and versican are differentially regulated following spinal cord injury. Exp Neurol 182:399–411
Juraska JM, Kopcik JR (1988) Sex and environmental influences on the size and ultrastructure of the rat corpus callosum. Brain Res 450:1–8
Kanesaka T, Mori M, Hattori T et al (2006) Serum matrix metalloproteinase-3 levels correlate with disease activity in relapsing-remitting multiple sclerosis. J Neurol Neurosurg Psychiatry 77: 185–188
Katayama Y, Becker DP, Tamura T et al (1990) Massive increases in extracellular potassium and the indiscriminate release of glutamate following concussive brain injury. J Neurosurg 73: 889–900

Kelley BJ, Lifshitz J, Povlishock JT (2007) Neuroinflammatory responses after experimental diffuse traumatic brain injury. J Neuropath Exp Neurol 66:989–1001
Kelso ML, Scheff NN, Scheff SW et al (2011) Melatonin and minocycline for combinatorial therapy to improve functional and histopathological deficits following traumatic brain injury. Neurosci Let 488:60–64
Kim JHY, Ellman A, Juraska JM (1996) A re-examination of sex differences in axon density and number in the splenium of the rat corpus callosum. Brain Res 740:47–56
Kim HJ, Fillmore HL, Reeves TM et al (2005) Elevation of hippocampal MMP-3 expression and activity during trauma-induced synaptogenesis. Exp Neurol 192:60–72
King AI, Ruan JS, Zhou C et al (1995) Recent advances in biomechanics of brain injury research: a review. J Neurotrauma 12:651–658
Kocsis JD, Waxman SG (1980) Absence of potassium conductance in central myelinated axons. Nature 287:348–349
Kordeli E, Bennett V (1991) Distinct ankyrin isoforms at neuron cell bodies and nodes of Ranvier resolved using erythrocyte ankyrin-deficient mice. J Cell Biol 114:1243–1259
Kordeli E, Lambert S, Bennett V (1995) AnkyrinG. A new ankyrin gene with neural-specific isoforms localized at the axonal initial segment and node of Ranvier. J Biol Chem 270: 2352–2359
Lamantia AS, Rakic P (1990) Cytological and quantitative characteristics of four cerebral commissures in the rhesus monkey. J Comp Neurol 291:520–537
Leker RR, Shohami E (2002) Cerebral ischemia and trauma: different etiologies yet similar mechanisms—neuroprotective opportunities. Brain Res Rev 39:55–73
Leppert D, Ford J, Stabler G et al (1998) Matrix metalloproteinase-9 (gelatinase B) is selectively elevated in CSF during relapses and stable phases of multiple sclerosis. Brain 121:2327–2334
Levin HS (1996) Neurobehavioral outcome of closed head injury: implications for clinical trials. In: Bandak FA, Eppinger RH, Ommaya AK (eds) Traumatic brain injury: bioscience and mechanics. Mary Ann Liebert, Larchmont, New York, pp 105–114
Li X-Y, Feng D-F (2009) Diffuse axonal injury: novel insights into detection and treatment. J Clin Neurosci 16:614–619
Li ZP, Burke EP, Frank JS et al (1993) The cardiac Na+-Ca2+ exchanger binds to the cytoskeletal protein ankyrin. J Biol Chem 268:11489–11491
Li RB, Guo XC, Liang HX et al (2009) Study on changes of MMP-3 expression after brain contusion in rats. Leg Med (Tokyo) 11(Suppl 1):S176–S179
Lin Y, Pan Y, Wang M et al (2012) Blood–brain barrier permeability is positively correlated with cerebral microvascular perfusion in the early fluid percussion-injured brain of the rat. Lab Invest 10:1038 [Epub ahead of print]
Liu H, Kim Y, Chattopadhyay S et al (2010) Matrix metalloproteinase inhibition enhances the rate of nerve regeneration in vivo by promoting dedifferentiation and mitosis of supporting schwann cells. J Neuropathol Exp Neurol 69:386–395
Lyeth BG, Jenkins LW, Hamm RJ et al (1990) Prolonged memory impairment in the absence of hippocampal cell death following traumatic brain injury in the rat. Brain Res 526:249–258
Malhotra JD, Koopmann MC, Kazen-Gillespie KA et al (2002) Structural requirements for interaction of sodium channel beta-1 subunits with ankyrin. J Biol Chem 277:26681–26688
Maller JJ, Thomson RH, Lewis PM et al (2010) Traumatic brain injury, major depression, and diffusion tensor imaging: making connections. Brain Res Rev 64:213–240
Marmarou CR, Povlishock JT (2006) Administration of the immunophilin ligand FK506 differentially attenuates neurofilament compaction and impaired axonal transport in injured axons following diffuse traumatic brain injury. Exp Neurol 197:353–362
Mathey EK, Derfuss T, Storch MK et al (2007) Neurofascin as a novel target for autoantibody-mediated axonal injury. J Exp Med 204:2363–2372
Matsukawa H, Shinoda M, Fujii M et al (2011) Genu of corpus callosum as a prognostic factor in diffuse axonal injury. J Neurosurg 115:1019–1024
Maxwell WL, Irvine A, Graham DI et al (1991) Focal axonal injury: the early axonal response to stretch. J Neurocytol 20:157–164

Maxwell WL, Watt C, Graham DI et al (1993) Ultrastructural evidence of axonal shearing as a result of lateral acceleration of the head in non-human primates. Acta Neuropathol 86: 136–144

Maxwell WL, Povlishock JT, Graham DL (1997) A mechanistic analysis of nondisruptive axonal injury: a review. J Neurotrauma 14:419–440

Mbye LH, Singh IN, Sullivan PG et al (2008) Attenuation of acute mitochondrial dysfunction after traumatic brain injury in mice by NIM811, a nonimmunosuppressive cyclosporin A analog. Exp Neurol 209:243–253

Mbye LH, Singh IN, Carrico KM et al (2009) Comparative neuroprotective effects of cyclosporin A and NIM811, a nonimmunosuppressive cyclosporin A analog, following traumatic brain injury. J Cereb Blood Flow Metab 29:87–97

Meighan PC, Meighan SE, Davis CJ et al (2007) Effects of matrix metalloproteinase inhibition on short- and long-term plasticity of schaffer collateral/CA1 synapses. J Neurochem 102: 2085–2096

Meythaler JM, Peduzzi JD, Eleftheriou E et al (2001) Current concepts: diffuse axonal injury-associated traumatic brain injury. Arch Phys Med Rehabil 82:1461–1471

Michaely P, Bennett V (1995) Mechanism for binding site diversity on ankyrin. Comparison of binding sites on ankyrin for neurofascin and the Cl−/HCO3− anion exchanger. J Biol Chem 270:31298–31302

Morganti-Kossmann MC, Satgunaseelan L, Bye N et al (2007) Modulation of immune response by head injury. Injury 38:1392–1400

Muir EM, Adcock KH, Morgenstern DA et al (2002) Matrix metalloproteases and their inhibitors are produced by overlapping populations of activated astrocytes. Brain Res Mol Brain Res 100:103–117

Murata Y, Rosell A, Scannevin RH et al (2008) Extension of the thrombolytic time window with minocycline in experimental stroke. Stroke 39:3372–3377

Nashmi R, Fehlings MG (2001) Changes in axonal physiology and morphology after chronic compressive injury of the thoracic spinal cord. Neuroscience 104:235–251

Newcomb JK, Kampfl A, Posmantur RM et al (1997) Immunohistochemical study of calpain-mediated breakdown products to a-spectrin following controlled cortical impact injury in the rat. J Neurotrauma 14:369–383

Noble LJ, Donovan F, Igarashi T et al (2002) Matrix metalloproteinases limit functional recovery after spinal cord injury by modulation of early vascular events. J Neurosci 22:7526–7535

Ochiai T, Nakajima K, Sakamoto K et al (1989) Comparative studies on the immunosuppressive activity of FK506, 15-deoxyspergualin, and cyclosporine. Transplant Proc 21:829–832

O'Connor WT, Smyth A, Gilchrist MD (2011) Animal models of traumatic brain injury: a critical evaluation. Pharmacol Ther 130:106–113

Okonkwo DO, Buki A, Siman R et al (1999) Cyclosporin A limits calcium-induced axonal damage following traumatic brain injury. Neuroreport 10:353–358

Pandya DN, Karol EA, Heilbronn D (1971) The topographical distribution of interhemispheric projections in the corpus callosum of the rhesus monkey. Brain Res 32:31–43

Park E, Liu E, Shek M et al (2007) Heavy neurofilament accumulation and alpha-spectrin degradation accompany cerebellar white matter functional deficits following forebrain fluid percussion injury. Exp Neurol 204:49–57

Park E, Bell JD, Baker AJ (2008) Traumatic brain injury: can the consequences be stopped? Canadian Med Assoc J 178:1163–1170

Park KP, Rosell A, Foerch C et al (2009) Plasma and brain matrix metalloproteinase-9 after acute focal cerebral ischemia in rats. Stroke 40:2836–2842

Partadiredja G, Miller R, Oorschot DE (2003) The number, size, and type of axons in rat subcortical white matter on left and right sides: a stereological, ultrastructural study. J Neurocytol 32:1165–1179

Peters LL, John KM, Lu FM et al (1995) Ank3 (epithelial ankyrin), a widely distributed new member of the ankyrin gene family and the major ankyrin in kidney, is expressed in alternatively spliced forms, including forms that lack the repeat domain. J Cell Biol 130:313–330

Pettus EH, Christman CW, Giebel ML et al (1994) Traumatically induced altered membrane permeability: its relationship to traumatically induced reactive axonal change. J Neurotrauma 11:507–522

Phillips LL, Reeves TM (2001) Interactive pathology following traumatic brain injury modifies hippocampal plasticity. Restor Neurol Neurosci 19:213–235

Pierpaoli C, Barnett A, Pajevic S et al (2001) Water diffusion changes in Wallerian degeneration and their dependence on white matter architecture. Neuroimage 13:1174–1185

Pomicter AD, Shroff SM, Fuss B et al (2010) Novel forms of neurofascin 155 in the central nervous system: alterations in paranodal disruption models and multiple sclerosis. Brain 133: 389–405

Povlishock JT (1992) Traumatically induced axonal injury: pathogenesis and pathobiological implications. Brain Pathol 2:1–12

Povlishock JT, Christman CW (1995) The pathobiology of traumatically induced axonal injury in animals and humans: a review of current thoughts. J Neurotrauma 12:555–564

Povlishock JT, Katz DI (2005) Update of neuropathology and neurological recovery after traumatic brain injury. J Head Trauma Rehabil 20:76–94

Povlishock JT, Marmarou T, McIntosh T et al (1997) Impact acceleration injury in the rat: evidence for focal axolemmal change and related neurofilament sidearm alteration. J Neuropathol Exp Neurol 56:347–359

Rasband MN, Peles E, Trimmer JS et al (1999) Dependence of nodal sodium channel clustering on paranodal axoglial contact in the developing CNS. J Neurosci 19:7516–7528

Reeves TM, Colley BS (2012) Electrophysiological approaches in traumatic brain injury. In: Chen J, Xu Z, Xu X-M, Zheng J (eds) Animal models of acute neurological injuries II: injury and mechanistic assessments. Humana Press, New York, pp 313–330

Reeves TM, Phillips LL, Povlishock JT (2005) Myelinated and unmyelinated axons of the corpus callosum differ in vulnerability and functional recovery following traumatic brain injury. Exp Neurol 196:126–139

Reeves TM, Phillips LL, Lee NN et al (2007) Preferential neuroprotective effect of tacrolimus (FK506) on unmyelinated axons following traumatic brain injury. Brain Res 1154:225–236

Reeves TM, Prins ML, Zhu J-P, Povlishock JT, Phillips LL (2003) Matrix metalloproteinase inhibition alters functional and structural correlates of deafferentation-induced sprouting in the dentate gyrus. J Neurosci 23:10182–10189

Reeves TM, Greer JE, Vanderveer AS et al (2010) Proteolysis of submembrane cytoskeletal proteins ankyrin-G and αII-spectrin following diffuse brain injury: a role in white matter vulnerability at Nodes of Ranvier. Brain Pathol 20:1055–1068

Reeves TM, Smith TL, Williamson JC et al (2012) Unmyelinated axons show selective rostrocaudal pathology in the corpus callosum following traumatic brain injury. J Neuropathol Exp Neurol 71:198–210

Romanic AM, White RF, Arleth AJ et al (1998) Matrix metalloproteinase expression increases after cerebral focal ischemia in rats: inhibition of matrix metalloproteinase-9 reduces infarct size. Stroke 29:1020–1030

Romero-Perez D, Fricovsky E, Yamasaki KG et al (2008) Cardiac uptake of minocycline and mechanisms for in vivo cardioprotection. J Am Coll Cardiol 52:1086–1094

Rosa CM, Luigi B, Antonio D et al (2011) Early prognosis after severe traumatic brain injury with minor or absent computed tomography scan lesions. J Trauma 70:447–451

Rosenberg GA, Sullivan N, Esiri MM (2001) White matter damage is associated with matrix metalloproteinases in vascular dementia. Stroke 32:1162–1168

Rubtsov AM, Lopina OD (2000) Ankyrins. FEBS Lett 482:1–5

Rushton WA (1951) A theory of the effects of fibre size in medullated nerve. J Physiol 115:101–122

Rutgers DR, Fillard P, Paradot G et al (2008) Diffusion tensor imaging characteristics of the corpus callosum in mild, moderate, and severe traumatic brain injury. AJNR Am J Neuroradiol 29:1730–1735

Rutland-Brown W, Langlois JA, Thomas KE et al (2006) Incidence of traumatic brain injury in the United States, 2003. J Head Trauma Rehabil 21:544–548
Saatman KE, Graham DI, McIntosh TK (1998) The neuronal cytoskeleton is at risk after mild and moderate brain injury. J Neurotrauma 15:1047–1058
Saatman KE, Abai B, Grosvenor A et al (2003) Traumatic axonal injury results in biphasic calpain activation and retrograde transport impairment in mice. J Cereb Blood Flow Metab 23:34–42
Saatman KE, Creed J, Raghupathi R (2010) Calpain as a therapeutic target in traumatic brain injury. Neurotherapeutics 7:31–42
Samorajski T, Friede RL (1968) A quantitative electron microscopic study of myelination in the pyramidal tract of rat. J Comp Neur 134:323–338
Scherer SS (1999) Nodes, paranodes, and incisures: from form to function. Ann N Y Acad Sci 883:131–142
Seggie J, Berry M (1972) Ontogeny of interhemispheric evoked potentials in the rat: significance of myelination of the corpus callosmn. Exp Neurol 35:215–232
Seo JH, Guo S, Lok J et al (2012) Neurovascular matrix metalloproteinases and the blood–brain barrier. Curr Pharm Des 18:3645–3648
Setkowicz Z, Guzik R (2007) Injections of vehicle, but not cyclosporin A or tacrolimus (FK506), afford neuroprotection following injury in the developing rat brain. Acta Neurobiol Exp 67:399–409
Shigemori Y, Katayama Y, Mori T et al (2006) Matrix metalloproteinase-9 is associated with blood–brain barrier opening and brain edema formation after cortical contusion in rats. Acta Neurochir Suppl 96:130–133
Sidaros A, Engberg AW, Sidaros K et al (2008) Diffusion tensor imaging during recovery from severe traumatic brain injury and relation to clinical outcome: a longitudinal study. Brain 131:559–572
Singleton RH, Stone JR, Okonkwo DO et al (2001) The immunophilin ligand FK506 attenuates axonal injury in an impact-acceleration model of traumatic brain injury. J Neurotrauma 18:607–614
Singleton RH, Zhu J, Stone JR et al (2002) Traumatically induced axotomy adjacent to the soma does not result in acute neuronal death. J Neurosci 22:791–802
Skandsen T, Kvistad KA, Solheim O et al (2010) Prevalence and impact of diffuse axonal injury in patients with moderate and severe head injury: a cohort study of early magnetic resonance imaging findings and 1-year outcome. J Neurosurg 113:556–563
Smith RS, Koles ZJ (1970) Myelinated nerve fibers: computed effect of myelin thickness on conduction velocity. Am J Physiol 219:1256–1258
Smith DH, Meaney DF (2000) Axonal damage in traumatic brain injury. Neuroscientist 6:483–495
Smith DH, Chen XH, Nonaka M et al (1998) Accumulation of amyloid beta and tau and the formation of neurofilament inclusions following diffuse brain injury in the pig. J Neuropathol Exp Neurol 58:982–992
Solé S, Petegnief V, Gorina R et al (2004) Activation of matrix metalloproteinase-3 and agrin cleavage in cerebral ischemia/reperfusion. J Neuropathol Exp Neurol 63:338–349
Srinirasan Y, Elmer L, Davis J et al (1988) Ankyrin and spectrin associate with voltage-dependent sodium channels in brain. Nature 333:177–180
Stone JR, Singleton RH, Povlishock JT (2000) Antibodies to the C-terminus of the beta-amyloid precursor protein (APP): a site specific marker for the detection of traumatic axonal injury. Brain Res 871:288–302
Stone JR, Singleton RH, Povlishock JT (2001) Intra-axonal neurofilament compaction does not evoke local axonal swelling in all traumatically injured axons. Exp Neurol 172:320–331
Stone JR, Okonkwo DO, Singleton RH et al (2002) Caspase-3-mediated cleavage of amyloid precursor protein and formation of amyloid Beta peptide in traumatic axonal injury. J Neurotrauma 19:601–614
Strich SJ (1961) Shearing of nerve fibers as a cause of brain damage due to head injury: a pathological study of twenty cases. Lancet 2:443–448

Sturrock RR (1980) Myelination of the mouse corpus callosum. Neuropathol Appl Neurobiol 6:415–420
Stys PK (2004) White matter injury mechanisms. Cur Mol Med 4:113–130
Susuki K, Rasband MN (2008a) Molecular mechanisms of node of Ranvier formation. Curr Opin Cell Biol 20:616–623
Susuki K, Rasband MN (2008b) Spectrin and ankyrin-based cytoskeletons at polarized domains in myelinated axons. Exp Biol Med 233:394–400
Suzuki Y, Nagai N, Umemura K et al (2007) Stromelysin-1 (MMP-3) is critical for intracranial bleeding after t-PA treatment of stroke in mice. J Thromb Haemost 5:1732–1739
Swanson TH, Krahl SE, Liu Y-Z et al (1998) Evidence for physiologically active axonal adenosine receptors in the rat corpus callosum. Brain Res 784:188–198
Thomalla G, Glauche V, Koch MA et al (2004) Diffusion tensor imaging detects early Wallerian degeneration of the pyramidal tract after ischemic stroke. Neuroimage 22:1767–1774
Thompson HJ, Lifshitz J, Marklund N et al (2005) Lateral fluid percussion brain injury: a 15-year review and evaluation. J Neurotrauma 22:42–75
Truettner JS, Alonso OF, Dietrich DW (2005) Influence of therapeutic hypothermia on matrix metalloproteinase activity after traumatic brain injury in rats. J Cereb Blood Flow Metab 25: 1505–1516
Vilalta A, Sahuquillo J, Rosell A et al (2008) Moderate and severe traumatic brain injury induce early overexpression of systemic and brain gelatinases. Intensive Care Med 34:1384–1392
von Reyn CR, Spaethling JM, Mesfin MN et al (2009) Calpain mediates proteolysis of the voltage-gated sodium channel alpha-subunit. J Neurosci 29:10350–10356
Walker EJ, Rosenberg GA (2009) TIMP-3 and MMP-3 contribute to delayed inflammation and hippocampal neuronal death following global ischemia. Exp Neurol 216:122–131
Wang KK (2000) Calpain and caspase: can you tell the difference? Trends Neurosci 23:20–26
Warren KM, Reeves TM, Phillips LL (2012) MT5-MMP, ADAM-10 and N-Cadherin act in concert to facilitate synapse reorganization following traumatic brain injury. J Neurotrauma 29:1922–1940
Waxman SG, Swadlow HA (1976) Ultrastructure of visual callosal axons in the rabbit. Exp Neurol 53:115–127
Wells JEA, Hurlbert RJ, Fehlings MG et al (2003) Neuroprotection by minocycline facilitates significant recovery from spinal cord injury in mice. Brain 126:1628–1637
Wójtowicz T, Mozrzymas JW (2010) Late phase of long-term potentiation in the mossy fiber-CA3 hippocampal pathway is critically dependent on metalloproteinases activity. Hippocampus 20:917–921
Wood SJ, Slater CR (1998) beta-Spectrin is colocalized with both voltage-gated sodium channels and ankyrin G at the adult rat neuromuscular junction. J Cell Biol 140:675–684
Wright JW, Brown TE, Harding JW (2007) Inhibition of hippocampal matrix metalloproteinase-3 and -9 disrupts spatial memory. Neural Plast 2007:73813
Xiong Y, Rabchevsky AG, Hall ED (2007) Role of peroxynitrite in secondary oxidative damage after spinal cord injury. J Neurochem 100:639–649
Yenari MA, Xu L, Tang XN et al (2006) Microglia potentiate damage to blood–brain barrier constituents. Stroke 37:1087–1093
Yong VW (2005) Metalloproteinases: mediators of pathology and regeneration in the CNS. Nat Rev Neurosci 6:931–944
Yong VW, Zabad RK, Agrawal S et al (2007) Elevation of matrix metalloproteinases (MMPs) in multiple sclerosis and impact of immunomodulators. J Neurol Sci 259:79–84
Zhang Y, Winterbottom JK, Schachner M et al (1997) Tenascin-C expression and axonal sprouting following injury to the spinal dorsal columns in the adult rat. J Neurosci Res 49:433–450
Zhao BQ, Wang S, Kim HY et al (2006) Role of matrix metalloproteinases in delayed cortical responses after stroke. Nat Med 12:441–445
Zhou D, Lambert S, Malen PL et al (1998) AnkyrinG is required for clustering of voltage-gated Na channels at axon initial segments and for normal action potential firing. J Cell Biol 143:1